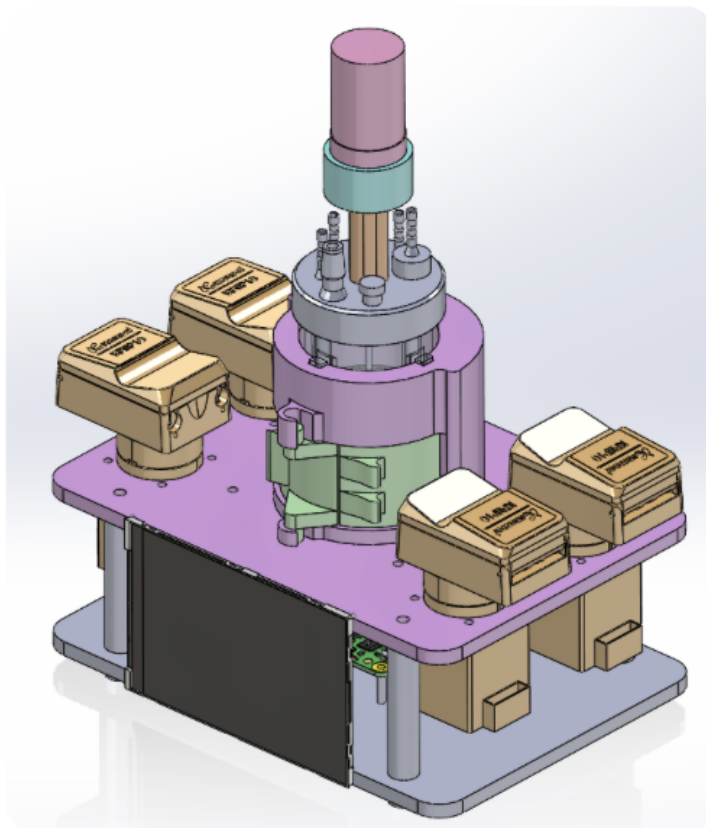


Non-Invasive Miniature Bioreactor for Laboratory Engineering (NIMBLE)



Course Instructor:
Douglas Hart

Communication Instructors:
Juergen Schoenstein, Jared Berezin

2.013 Fall 2024 Team:

Reyna Ayala, Gerardo Berlanga Molina, Timber Carey, Rakibul Chowdhury, Christian Duessel, Faris Elnager, Abraham Lemaitre, Sehar Lohawala, Henry Smith, Miguel Talamantez

December 10, 2024

Contents

Executive Summary	2
1 Project Overview	5
1.1 Motivation	5
1.2 Goals	7
1.3 System Design Requirements	7
1.4 Design Overview	8
2 Heating System	10
2.1 Determining Ranges and Tolerances of Temperature Control	10
2.2 Steady-State Heating Power Consumption	10
2.3 Peak Power Consumption	11
2.4 Heater Selection	12
2.5 Thermal Time Constant Quantification	12
2.6 Thermal Gradient Within the Vessel	13
2.7 Safety and Thermal Insulation	13
3 Fluid Flow & Agitation System	16
3.1 Determining Desired Range for Feed and Output Rates	16
3.2 Agitation Rate Expected Range	16
3.3 Selection of Stirring Method	17
3.4 Evaluating Flow Speed in Sensing Trenches Using Fluid Simulations	18
3.5 Using Fluid Simulations to Assess Mixing	20
3.6 Simulated Oxygen Transfer from Agitation	23
4 Sensors	24
4.1 Temperature Sensor	24
4.1.1 Temperature Sensor Working Principle	24
4.1.2 Temperature Sensor Circuit Design Considerations	25
4.2 pH Sensor	26
4.2.1 pH Sensor Working Principle	26
4.2.2 NIMBLE's pH Sensor	27
4.2.3 pH Amplifier Circuits	28
4.3 Dissolved Oxygen Sensor	31
4.3.1 Dissolved Oxygen Working Principle	31
4.3.2 NIMBLE's Dissolved Oxygen Sensor	32
4.3.3 DO Amplifier Circuits	33
4.4 Optical Density Sensor	37
4.4.1 OD Working Principle	37
4.4.2 NIMBLE's OD Sensor	38
4.4.3 OD Analysis	39
4.4.4 OD Amplifier Circuits	40
4.5 Sensors Calibration	40
4.6 Sensors Testing	42
4.6.1 pH Polyaniline (PANI) Layer	42
4.6.2 DO Ruthenium Layer	51
5 Electronics	53
5.1 Power Electronics	53
5.2 Gate Drivers	54
5.3 Analog Signal Input, Data, and Filtering	57

6 Environment Control	60
6.1 Temperature Control	60
6.2 pH Control	62
6.3 Dissolved Oxygen Control	63
6.4 Environment Control Future Work	63
7 Vessel and Structure Design	65
7.1 Reaction Vessel Overview	65
7.1.1 Basic Geometry	65
7.1.2 Trenches	66
7.1.3 Lid	66
7.1.4 Material Selection	67
7.2 Reusable Base	70
7.2.1 Overview	70
7.2.2 Vessel Heater	70
7.2.3 Sensor Packaging	71
8 Bill of Materials	72
9 Future Work	74
9.1 Remaining Risks	74
9.2 Remaining Design Work	74
9.3 Remaining Testing	75
10 Acknowledgments	76
11 References	77
Appendices	78
A Thermodynamics Calculations MATLAB Script	79
B Shear Calculations	80
C Sensors Calulcations MATLAB Script	81

Executive Summary

The Non-Invasive Miniature Bioreactor for Laboratory Engineering project, better known as NIMBLE, aims to develop an innovative 100mL small-scale lab bench bioreactor that bridges the gap between what's in demand for bioreactors and what's currently available on the market. This product uses a low-cost reusable system that is meant for long term use in conjunction with an even lower-cost non-reusable vessel that allows users to avoid sanitary processes and concerns with contamination. The product features non-invasive sensing capabilities for pH, Optical Density (OD), Dissolved Oxygen (DO), and temperature as well as feedback control systems for pH, DO, and temperature. The system is designed to operate for 2 weeks before a new vessel needs to be used. NIMBLE has several innovative features such as a custom optical sensing architecture used for the OD, DO, and pH measurements. The design uses both a ruthenium-based layer and a polyaniline-based layer placed internally to allow for purely non-invasive optical sensing. This product will serve as a general-use bioreactor for a broad range of applications in laboratories using its ability to maintain such custom conditions with easily disposable vessels.

NIMBLE is 227mm tall and 190mm wide to give it a portable, compact design. It's designed to be implemented as a small-scale continuous bioreactor and provide the ability to work in parallel with more of itself if needed with its small dimensions. The bioreactor comprises reusable components such as sensors and the primary structure, and non-reusable components such as the vessel. The intention behind non-reusable components is to allow the user to quickly and effectively start a new procedure with as minimal work as possible. This system also prevents potential contamination between procedures.

One of the primary requirements of the bioreactor is its ability to sustain a stable temperature which was decided to be between 25°C and 50°C. This range of heating ability was determined both from market research and was given to us by our sponsor, Todd Thorsen. We performed calculations using a thermal resistance model to determine how much heat the bioreactor vessel would dissipate to the environment to calculate power consumption. After investigating methods to heat our vessel, we decided to implement a flexible silicone rubber heating pad placed on the sides of our cylindrical vessel. Given that we are heating our vessel from the outside as opposed to an internal heating mechanism, we supported this decision by calculating a time constant of temperature change of about 20 seconds. This means the bioreactor can control temperature fluctuations with a 20 second delay. Another conclusion we made was that due to the small dimensions of our vessel, thermal gradient can be considered negligible and is supported in greater detail in our calculations. Due to our ability to sustain high temperatures, thermal insulation is required to not only provide protection for the user, but to prevent excess heat from leaving the system. This insulation is implemented as a 2mm flexible Teknofibra insulation layer.

In typical bioreactors, agitation is critically required to allow processes to occur with the live culture that is present. This can be implemented with a stir mechanism of some kind, vibration, or vessel movement. Due to innovative sensor technology in NIMBLE, the vessel is not shaped as straightforward as usual and requires ensuring homogeneity of the fluid in order to consider measurements to be representative of the rest of the vessel. This is accomplished with a custom impeller design which forces flow through the abnormal crevices of the vessel. Additionally, fluid simulations were done to confirm this agitation design would successfully flow fluid as needed, reach the desired speed requirements, and ensure needed oxygen transfer can occur.

The bioreactor's sensing system consists of four sensor packages: temperature, pH, dissolved oxygen (DO), and optical density (OD). These four measurements are taken using a unique "trench" method which involves custom shaped protrusions at the base of the vessel to allow light to be shown through the broth at a small scale. These sensing methods are completely non-invasive to the inside fluid and allow a unique opportunity as very few bioreactors offer sensing that does not come in contact with the fluid in any way. In this sensing system, there are two different layers used for sensing that are critical to allow for only optical sensing. A Polyaniline layer is implemented for pH sensing and a Tris Ruthenium(II) Complex layer is implemented for dissolved oxygen measurements. To sense temperature, a thermistor is placed on the bottom exterior of the vessel. Although it is on the exterior surface of the vessel, calculations were made to show that a time constant of approximately 30 seconds allows us to ensure this method of measurement is reliable enough. Before usage of any of these sensors, a calibration is used to ensure the reliability of data collected. A detailed procedure is followed using deionized water and a solution of known pH. To best design this innovative sensor package, testing was also conducted to create these layers and ensure their accuracy and needed conditions. Although complete experimentation was left unfinished, there is detailed

documentation on how to go about creating these layers successfully.

Using a Raspberry Pi, a custom PCB, and a laptop power adapter, the bioreactor is able to perform its sensing capabilities, sensoring feedback control, and physical manipulation such as motors and its heating mechanism. The bioreactor uses a custom PCB to perform power electronics needed to step down wall outlet voltage to 12V and 5V as needed for logic components and for power consuming features. At equilibrium power consumption, the bioreactor runs off of approximately 16W (primarily towards heating). To manipulate the heating mechanism, the motors, and pumps, the Raspberry Pi uses a series of gate drivers to control a MOSFET configuration. Additionally, filtering circuitry is implemented on the PCB to do noise reduction and signal processing before reaching the analog pins of the Raspberry Pi.

To control the various conditions in the vessel such as temperature, pH, cell density, and dissolved oxygen, each condition has a dedicated controller designed according to its specifications. The goal of the control scheme is to achieve complete autonomy while meeting all conditions at all times. To achieve temperature control, a thermal resistance model is used to support the implementation of a PI controller. To achieve pH control, a closed-loop feedback on-off controller is used given the long time delay in measurements. To achieve dissolved oxygen control, the system also utilizes a closed-loop feedback on-off controller.

Structurally, the base holds the electronics, the disposable reaction vessel, and the pumps. The custom vessel highlights a “trench” sensor design, side flanges to allow for improved fluid agitation, and a sealed lid which features a keyed connection for a motor to connect to the stir bar. The vessel uses Nylon-12 and suggests using a Formlabs Bioresin for prototyping.

1 Project Overview

1.1 Motivation

Small-scale bioreactors can be found across many different biomedical, pharmaceutical, biological, and chemical applications. These applications can be for things such as fermentation of yeast or the manipulation of blood cells. However, there is a very large gap in the bioreactor market between what is offered, and what is needed.

What's common among these various uses of bioreactors is that there is very rarely a case where a laboratory can buy a bioreactor and need not modify it to their custom needs, which we saw first-hand both on the MIT campus and in industry. In some cases this means modifying the system from perfusion continuous flow to chemostat continuous flow, while in others, it means physically modifying the vessel in order to take additional measurements the bioreactor doesn't perform. This trend of jerry-rigging bioreactors is both highly inconvenient and a risk to the performance of the bioreactor and its products.

Through both online and in-person research, we examined several different bioreactors available on the market. First, we looked at general large-scale bioreactors (Fig. 1a). While these often have advanced sensing capabilities, they are very expensive and require extensive sanitation processes. We then examined a much smaller scale bioreactor, the Pioreactor, that we were able to purchase in order to study it more thoroughly (Fig. 1b). This bioreactor was very low-cost, but its sensing capabilities were inadequate and it was not single-use, which could introduce contamination in successive processes. By visiting Ginkgo Bioworks, we were introduced to Sartorius's single-use lab-scale bioreactors (Fig. 1c). While this product had good sensing capabilities and was generally pretty low-cost, the users had to jerry-rig the perfusion device for chemostat applications. Finally, we examined Eppendorf's single-use bioreactors, which had very similar features to those of Sartorius but were less cost-effective (Fig. 1d). We collected all of this information to determine where our product will fit in the market, and a thorough comparison is laid out in Table 1.



(a) 5L-30L reusable bioreactor (Sartorius). (b) 20mL miniature bioreactor (Pioreactor).



(c) 250mL single-use bioreactor (Sartorius).

(d) 100mL-40L single-use bioreactors (Eppendorf).

Figure 1: Various bioreactors currently on the market. None meet all of the common needs of users.

Table 1: The niche in which we fit into the market. Compared to other single-use bioreactors, only NIMBLE provides all of the major sensing needs of users at this scale.

NIMBLE	General Large-Scale	Pioreactor 20mL	Sartorius Single-Use 250mL	Sartorius Benchtop 1L-10L	Eppendorf Single-Use 100mL-40L
Low-cost (reuse)	✓	✗	✓	✓	✗
Single Use	✓	✗	✗	✓	✓
Temp sensing and control	✓	✓	✓	✓	✓
pH sensing and control	✓	✓	✗	✓	✓
DO sensing and control	✓	✓	✗	✓	✓
OD sensing	✓	✓	✓	✓	✓
Perfusion Continuous Flow	✓	✓	✗	✓	✓
Chemostat Continuous Flow	✓	✓	✗	✗	✗
100% non-invasive sensing	✓	✗	✓	✗	✗
Lab-scale (~100mL)	✓	✗	✓	✓	✓
Data Logging	✓	✗	✓	✗	✗

1.2 Goals

The primary objective of this product is to meet the needs of users of bioreactors who are forced to modify existing products. Users who are doing experiments that contain highly sensitive processes desire a single-use vessel. This would allow them to, instead of spending significant amounts of time cleaning their bioreactor, exchange the vessel with a new one to avoid contamination and save time. Users also want the ability to have feedback in their system to maintain a steady pH, temperature, or dissolved oxygen concentration. Although this is common among bioreactors in use now, almost no bioreactors allow purely non-invasive sensing. Using a bioreactor with purely non-invasive sensing would allow for significantly faster and safer usage when dealing with sanitary-sensitive processes. Additionally, different processes require different methods of product production. This can be through use of a chemostat bioreactor system or a perfusion bioreactor system. Bioreactors very rarely have both of them in one product and when they do, they can cost upwards of \$50,000. This product is designed with both of these systems, as one of the primary goals is to be as general as possible to meet the demands of as many users as possible. The overall goal of this product is to meet the various needs of users to provide a bioreactor that is as general as possible and highly accessible. Bioreactors tend to be very expensive and very specific, so this product is meant to stray away from this to provide users with a suitable, low-cost, small-scale, and simple product they can use for whatever process they need.

1.3 System Design Requirements

We were provided with several design requirements from our sponsor, and as a team we decided on many others based on further research. These requirements are divided into three categories: basic functionality, user experience, and cost. Basic functionality and cost are hard requirements, while some user experience requirements are hard and some are softer.

Basic functionality requirements include sensing and control, structural considerations, and reaction process concerns. We need to be able to sense temperature, optical density, dissolved oxygen, and pH in order to monitor the reaction process. It is also critical to control temperature, dissolved oxygen, and pH within specific ranges to maintain the health of the culture. The vessel must be leak and ingress proof to prevent contamination, and have a possible run time of 2 weeks, which is a typical upper bound for production. Furthermore, the bioreactor should have a volume of 100 mL, which is the preferable minimum size for continuous feed and scalability, and should support continuous feed to enable longer-term production and steady-state conditions. These basic functionality requirements are laid out with quantitative metrics in Table 2.

Table 2: Basic functionality requirements.

Basic Functionality (Hard Req.)			
Requirement	Metric	Justification	Source
Temperature control	25°C-50°C ± 1°C	Critical to culture health	Sponsor
Optical density sensing	0-2 ± 0.1au	Needed to monitor culture growth stage	Sponsor
Dissolved oxygen sensing	2-10 mg/L	Need to monitor gas content	Team
pH sensing	4-9	Critical to culture health	Sponsor
Leak and ingress proof	IP68	Critical to prevent contamination	Team
Size - Benchtop scale	100 mL	Preferrable minimum size for continuous feed and scalability	Sponsor
Continuous Feed (Soft Req.)	0.1 - 5 mL/min	Enables longer-term production and steady state conditions	Team
Run time	2 weeks	Typical upper bound for production	Sponsor

User experience requirements have to do with the way the user interacts with the system. The user must have the ability to input parameters in order to control the reaction. The system should also be safe to interact with to prevent injury from excessive temperature or sharp objects, as well as portable so that the user can easily move it around their work environment. Additionally, there should be a real-time display of the sensed parameters, and the sensing data should be stored for post run-time analysis. These user experience requirements are summarized in Table 3.

In terms of cost, the whole system should be less than \$1000 to be competitive with other products on the market (Table 4). Some other single-use bioreactors are sold for several hundred dollars, while many larger-scale reusable bioreactors are sold for tens of thousands.

Table 3: User experience requirements.

User Experience			
Hard/Soft	Requirement	Metric	Source
Hard	Ability to input parameters	N/a	Team
Hard	Safety	<60°C surfaces, no sharp objects	Team
Soft	Real-time display of parameters	N/a	Team
Soft	Data logging	N/a	Team
Soft	Portable	<50 lbs	Team

Table 4: Cost requirements.

Cost (Hard Req.)		
Requirement	Metric	Source
Overall cost	<\$1000	Team

1.4 Design Overview

The NIMBLE system consists of seven primary systems: pumping, agitation, heating, vessel and base structures, sensors and electrical as seen in Figure 2. Microorganisms require a stable environment in order to continue producing high quality products such as proteins, lipids or ethanol. The entire system is designed to fit onto a lab bench as shown in Figure 3.

Our continuous-feed bioreactor continuously adds necessary food and nutrients to the vessel through the pumping system. The pumping system also removes waste and product during operation. The pumping system is also responsible for regulating pH levels in the vessel. There are four pumps: one for food inlet, one for waste/product output, one for acid addition and one for base addition.

The heating system maintains a stable temperature in the vessel using a resistive heat pad. The top portion of the vessel is exposed for passive cooling during the reaction.

To ensure homogeneity of temperature, biomass concentration and gas concentration, the agitation system continuously mixes the vessel. An external, reusable motor attaches to a disposable impeller shaft on the lid to mix the media inside the vessel.

The structures which support the systems are primarily 3d printed for prototyping but will be injection molded for mass manufacturing. The vessel is made of nylon-12 which has been specced to be both biocompatible and meet the light absorbance requirement of our optical sensors.

The sensor package is the innovation of our system. The sensors are fully optical, reusable and low cost. The system consists of four sensors measuring temperature, optical density, pH and dissolved gas. Novel coatings invented in academia are used on the interior of the vessel to react with changing pH and DO levels. LEDs shine light through representative samples located at the bottom of the vessel and the reflected light is measured by photodiode. The signal picked up by the photodiodes is correlated to known pH and DO levels to give accurate readings.

The electrical system consists of a Raspberry Pi and a custom PCB to input power from a standard US wall outlet into the bioreactor and control the systems. The Raspberry Pi controls the LED screen user interface, pumps, heater, sensors and agitation.

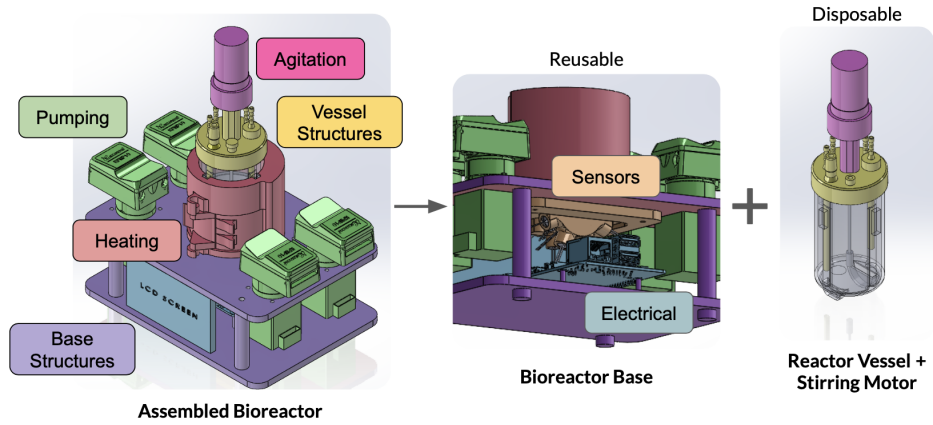


Figure 2: Overview of the bioreactor systems. NIMBLE consists of reusable and disposable parts to lower overall cost and minimize recurring costs.

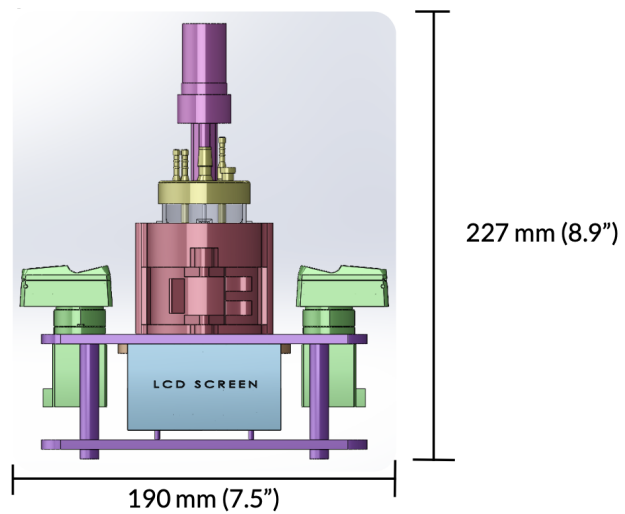


Figure 3: Overall dimensions of bioreactor. The small-scale requirement is meant for the system to fit on a lab bench.

2 Heating System

Bacteria and cells of interest typically have a narrow range of temperatures within which they can survive. Moreover, the specific ideal temperature for growth and production depends heavily on the bacteria or cell species and the reaction that is being performed. Therefore, it is vital for a general purpose bioreactor to be able to reach a large array of temperatures. To achieve this, we designed NIMBLE to have a temperature control range from 5°C above room temperature, i.e. 25°C, to 50°C. We do this using a flexible heating pad wrapped around the vessel that is able to apply at most 25W.

This section describes and justifies the analysis that we performed to justify the design decisions behind the heating system.

2.1 Determining Ranges and Tolerances of Temperature Control

In order to quantify the necessary temperature ranges and tolerances, we spoke to our sponsor, Todd Thorsen, and researched the temperature specifications of similar-scale bioreactors in the market.

Based on his experience with bioreactors, our sponsor suggested that our bioreactor should be able to hold the temperature set point within $\pm 0.5^\circ\text{C}$, which has been corroborated by the specifications we found. The findings from our market research are summarized in the table below.

Table 5: Bioreactor Temperature Ranges and Tolerances

Bioreactor	Temperature Range ($^\circ\text{C}$)	Tolerance ($^\circ\text{C}$)
C.NEST [4]	25 - 45	± 0.2
Ambr 250 [30]	18 - 55	± 0.5
Pioreactor [25]	20 - 50	No Spec
Biostat B [31]	0 - 80	± 0.1

We found that many bioreactors control temperature between room temperature, which we are considering to be 20°C, and approximately 50°C. The only bioreactor that went beyond these bounds on both directions was Sartorius' Biostat B. However, that bioreactor is of a slightly larger scale, 2.6L, compared to the other three which are closer to our volume of 100mL. This research also corroborated the acceptable temperature fluctuations that Todd determined we should be able to hold within. Thus, we decided to set the NIMBLE's temperature design requirement to be $25 - 50 \pm 0.5^\circ\text{C}$. To further verify the validity of this design requirement, we researched the optimal temperature for yeast fermentation, a common reaction that is performed in bioreactors. We found that yeast grows best at temperatures between 32 - 37°C, right in the heart(center?) of our desired temperature control [3].

2.2 Steady-State Heating Power Consumption

With a target temperature range in place, a heating method could be selected. First, we wanted to quantify how much heat the bioreactor vessel would dissipate to the environment at the maximum temperature of 50°C. This would tell us what the maximum power input would have be at steady state.

Heat loss is proportional to the difference in temperature between the ambient and the wall surface temperature. The analysis was done using a thermal resistance network.

The governing equation used to calculate power loss is:

$$\dot{Q} = \frac{\Delta T}{R_{tot}} \quad (1)$$

Here, $\Delta T = T_{wall} - T_{ambient}$. The temperature of the inside wall of the vessel was assumed to be the same as the maximum temperature of the solution, 50°C, and the ambient temperature of the air was assumed to be room temperature, 20°C. Therefore, $\Delta T = 30^\circ\text{C}$. Because the “resistors” are in series, the total resistance is calculated as:

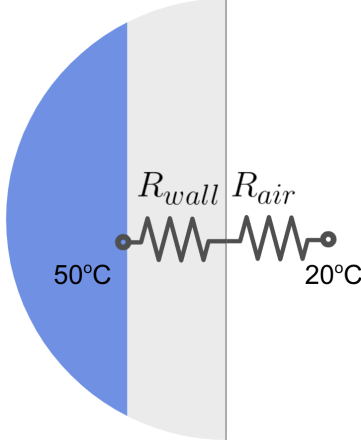


Figure 4: Thermal Resistance network used to quantify the worst-case-scenario power loss at maximum temperature. The thermal resistance of the wall was calculated using the equation $R_{wall} = \frac{L}{k_{Nylon12} \cdot SA}$, with $k_{Nylon12} = 0.14\text{W/m}^\circ\text{C}$ [19], $L = 0.002\text{m}$, and the maximum possible surface area, SA , for 100mL which is 0.013m^2 . The Thermal resistance for natural convection to the ambient air was calculated using $R_{air} = \frac{1}{h_{air} \cdot SA}$, with $h_{air} = 50\text{W/m}^2 \cdot ^\circ\text{C}$ [8], and the same surface area as before. The temperature of the wall on the inside of the vessel is assumed to be the same as the water at 50°C , and the ambient temperature is 20°C .

$$\begin{aligned} R_{tot} &= R_{wall} + R_{air} \\ &= \frac{L}{k_{Nylon12} \cdot SA} + \frac{1}{h_{air} \cdot SA} \end{aligned} \quad (2)$$

To get a worst-case-scenario calculation, the surface area, SA , of the vessel was initially taken to be the maximum it could be for a volume of 100mL. The shape that fulfills this requirement is a cube which would yield $SA = 0.013\text{m}^2$. Plugging in the thermal conductivity of Nylon 12, $k_{Nylon12} = 0.14\text{W/m}^\circ\text{C}$ [19], the thickness of the wall, $L = 0.002\text{m}$, the heat transfer coefficient of still air, $h_{air} = 50\text{W/m}^2 \cdot ^\circ\text{C}$ [8], and the calculated surface area, the total resistance is $R_{tot} = 2.6^\circ\text{C/W}$. Therefore, at maximum temperature, the power loss is:

$$\dot{Q} = \frac{30^\circ\text{C}}{2.6^\circ\text{C/W}} = 11.5\text{W}$$

2.3 Peak Power Consumption

From researching other bioreactors and consulting with people in labs who employ the same, we found that the typical amount of time that the user has to wait for the bioreactor to heat up is approximately 10 minutes. This metric dictates how much power the heater pulls at its peak, that is, when it is trying to create the impart the most energy to the vessel to raise its temperature from room temperature up to the reaction's set point.

To calculate the peak power, we considered how much energy it takes to change the full volume of water by 30°C . The governing equation comes from the first law of thermodynamics assuming a closed system:

$$\Delta E = Q - W \rightarrow \Delta E = Q \quad (3)$$

Then, the constitutive relationship for incompressible liquids, in this case water, shows that the heat transfer is equal to:

$$Q = mc_w\Delta T \quad (4)$$

With $m = 0.1\text{kg}$, and the specific heat capacity of water, $c_w = 4,184 \text{ J/kg}\cdot\text{°C}$. Thus, it would take 12kJ of energy to achieve our maximum desired temperature when starting from room temperature. To impart 12kJ of energy in 10 minutes, the heater must provide 20W of power.

2.4 Heater Selection

We selected a flexible silicone rubber heating pad to provide the necessary power to the vessel. The heating pad is 12.7cm \times 2.54cm (5" \times 1") and provides $0.78\text{W}/\text{cm}^2$ (5W/in²) which yields 25W total. Through our research into agitation, we discovered that the best aspect ratio (height to width) for bioreactors is 2:1. Therefore, for a volume of 100mL = 100cm³, our bioreactor had to have a diameter of 4cm and a height of 8cm as shown below.

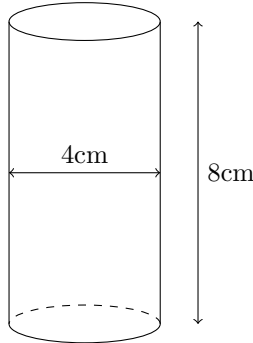


Figure 5: Dimensions of bioreactor vessel in centimeters.

These dimensions give a bottom surface area of $\pi \times (2\text{cm})^2 \approx 12.6\text{cm}^2$. This is quite constraining, especially considering the team's design choice to add "trenches" on the bottom of the vessel for non-invasive sensing purposes. The cylinder has a circumference of $\pi \times 4\text{cm} \approx 12.6\text{cm} \approx 5\text{in}$. Therefore, the heater would be mounted on the sides. To ensure proper thermal contact, this heating pad should be firmly attached to the edge of the vessel. The selected heating pad has an adhesive back which attaches to a 3D printed clamp that is secured with an elastic.

2.5 Thermal Time Constant Quantification

The time constant for the temperature of the outside of the bioreactor chamber wall to reach 63% of a step change in temperature of the water in contact with the inside of the chamber wall is approximately 20s. This is within the spec that we wish to control temperature fluctuations.

Due to the performance enhancements provided by non-invasive sensing, we placed the temperature sensor on the outside of the bioreactor vessel. This raised competing desired thermal characteristics: It is ideal to have a well-insulating chamber that reduces thermal heat loss to the environment—increasing heating and therefore, power efficiency—but not so well insulated that, by the time the temperature of the outside wall changes, it is no longer representative of the inner wall temperature. Thus, the vessel's time constant is an important metric to calculate.

A system's time constant τ depends on the material's density ρ , specific heat capacity c , its heat transfer coefficient h , and the volume V and cross-sectional area of interest A . The formula is:

$$\tau = \frac{\rho V c}{h A} \quad (5)$$

Dissecting the volume into $V = At$ with t the thickness of the wall, in this case 1mm, the formula becomes:

$$\tau = \frac{\rho A t c}{h A}$$

We noticed that $\rho A t c$ is the thermal capacitance C of the system [39]. Dissecting further, we saw that $1/(hA)$ is the thermal resistance R of the system. In this case we considered conduction, so $1/(hA)$ was re-written

as $t/(kA)$, with k the thermal conductivity of the vessel material, and again thickness t . Equation 5 then becomes:

$$\tau = RC = \frac{t}{kA} \times \rho Atc = \frac{\rho t^2 c}{k}$$

Therefore, the time constant becomes independent of the cross sectional area being considered, and is only a function of material properties and thickness.

Table 6: Material properties and their values [19].

Material Property	Symbol	Value
Density	ρ	1,260 kg/m ³
Specific Heat Capacity	c	2,130 J/(kg · m ³)
Thermal Conductivity	k	0.14 W/(m · °C)

Plugging in these values into our equation from before, we find that the time constant is:

$$\tau = \frac{1260 \text{ kg/m}^3 \times (0.001 \text{ m})^2 \times 2130 \text{ J/(kg} \cdot \text{m}^3)}{0.14 \text{ W/(m} \cdot \text{°C)}} \approx 20\text{sec}$$

Our specifications state that we want to control temperature fluctuations within 30s, therefore using this material, Nylon 12, we are able to detect these fluctuations in time, and our control system can take them into account in the feedback loop. Therefore, Nylon 12 was found to be an acceptable manufacturing material for the vessel from a thermal standpoint.

2.6 Thermal Gradient Within the Vessel

A concern with not heating the entire lateral surface area of the bioreactor was that there would be a large thermal gradient between the heated portion of the vessel and the ends of the vessel. To quantify this we calculated the heated surface area to volume ratio of the bioreactor:

$$\frac{\text{Unheated Surface Area}}{\text{Volume}} = 0.68\text{cm}^{-1} \quad (6)$$

This is a fairly low ratio which told us that the system will not be transferring a lot of heat to the environment, and this thermal gradient will not be an issue. Therefore, stirring the vessel will be enough to homogenize the temperature of the broth.

2.7 Safety and Thermal Insulation

The bioreactor design uses a 2mm thick insulation layer between the heater and the clamping mechanism. This layer has an adhesive side and is made of flexible Teknofibra insulation [9].

The heating method for our design is a heat pad that is wrapped around the outside of the vessel. This heating pad has an adhesive side that attaches directly to the clamping mechanism. This clamp is actuated by the user, which means that they will be in direct contact with a heated component. This raises a safety concern, so we designed a thermal barrier. The Teknofibra manufacturer provides some material properties on their site, as well as some testing data that they've found empirically. However, they do not provide the time constant of the material, so this was reverse engineered from their testing data.

On their website, the manufacturer specifies that they heated the material from 35°C to 310°C, and it took 300s for the temperature to stabilize. The governing equation is:

$$T_f = T_\infty + [T_i - T_\infty]e^{-t/\tau} \quad (7)$$

It was assumed that the stabilization temperature was 95% of the final 310°C, $T_f = 0.95 \times 310^\circ\text{C} = 294.5^\circ\text{C}$. The stabilization time t is 300s as specified by the manufacturer, and $T_i = 35^\circ\text{C}$ and $T_\infty = 310^\circ\text{C}$. Solving for τ , the equation becomes:

$$\tau = \frac{-t}{\ln\left(\frac{T_f - T_\infty}{T_i - T_\infty}\right)} \quad (8)$$

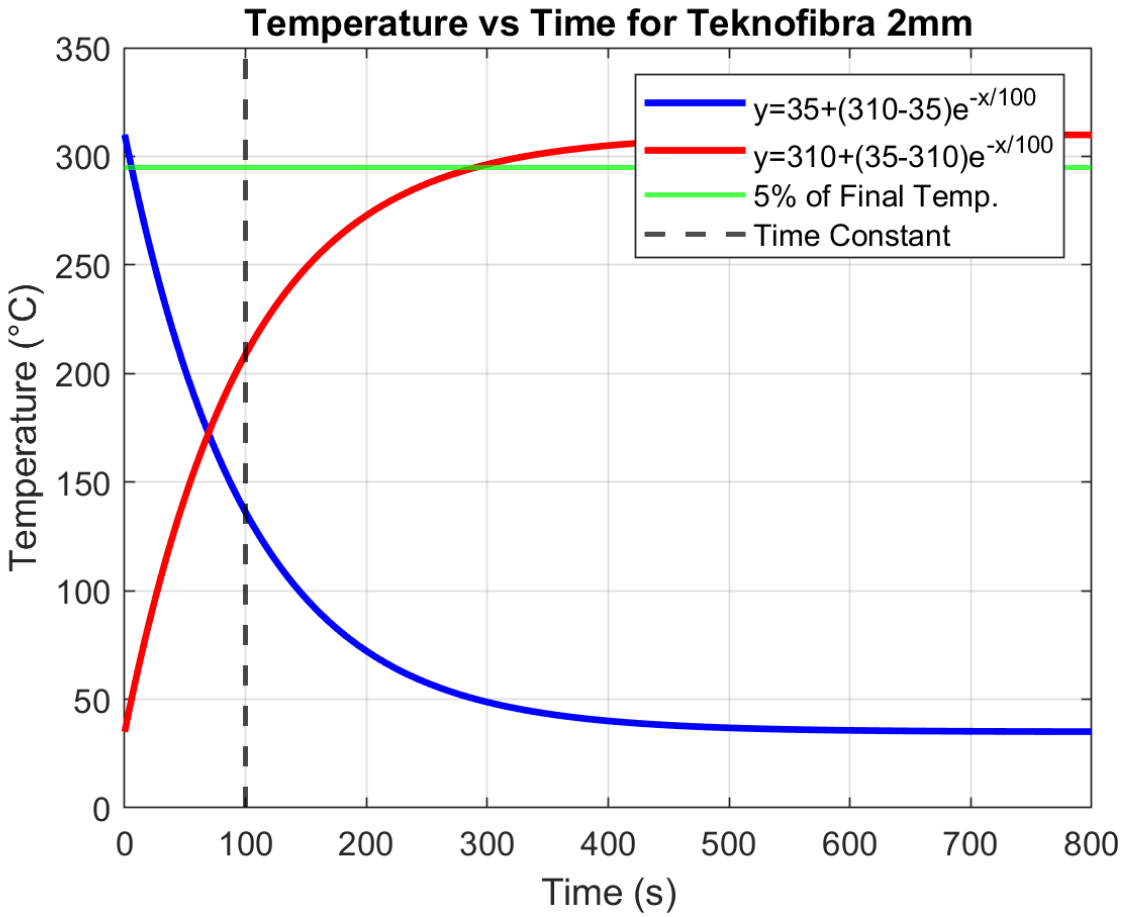


Figure 6: Reverse Engineering of Teknofibra's time-constant. The red line shows heating from 35°C to 310°C. The blue line shows cooling between the same two temperatures. The stabilization time was assumed to mean reaching 95% of the final temperature, indicated by the green line. The grey dashed line represents the thermal time constant of 100s.

Plugging in all respective values, $\tau \approx 100\text{s}$ as shown in Fig. 6.

For the rest of the bioreactor that is exposed, we determined that the temperature at the wall is only 38°C. Since this is nearly the same as body temperature, we decided that this was within our specification of safety.

To calculate the temperature at the wall, We had to find a more accurate rate of heat transfer through the wall. To achieve this, we used the radial conduction resistance. This is given by:

$$R_{cond} = \frac{\ln(r_{out}/r_{in})}{2\pi k H} \quad (9)$$

Here, $r_{out} = 0.022\text{m}$, $r_{in} = 0.02\text{m}$, and $H = 8\text{cm}$, with k as before. Therefore $R_{wall} = 1.4^\circ\text{C/W}$. For the thermal resistance of the convection to air, the Surface Area SA becomes $2\pi H r_{out} = 0.01\text{m}^2$ meaning that $R_{air} = 2^\circ\text{C/W}$. Using equation 1, the heat transfer was recalculated to be 8.9W. To find the outer wall temperature, the thermal resistance network was modified to only include the resistance of convection. Expanding ΔT into $T_{in} - T_{out}$ and solving equation 1 for T_{out} , this becomes:

$$T_{out} = T_{in} - \dot{Q} R_{wall} \quad (10)$$

Plugging in the appropriate values, we found that the temperature on the outer face of the bioreactor

vessel was 38°C. Further, we applied the same analysis to the heated sleeve to make sure that the insulation truly provided the safety we sought.

At peak power, the heater outputs a maximum of 25W. This was used to calculate the temperature that the heater would reach when the water reaches 50°C, the maximum target temperature. The thermal resistances of all the relevant components are summarized in the table below.

Table 7: Thermal Resistances of Various Components

Component	Thermal Resistance (°C/W)
R_{wall}	4.3
$R_{insulation}$	19.5
R_{clamp}	3.3
R_{air}	4.5

Solving equation 9 for T_{in} because the direction of heat exchange is opposite, the temperature of the heater was calculated to be 157.5°C. Then, using equation 1 with $\Delta T = 137.5^\circ\text{C}$ between the heater and the ambient air, and the total resistance of all the components in series $R_{tot} = 27.3^\circ\text{C}/\text{W}$, the outgoing power was calculated to be 5W. Using equation 9 one final time, the temperature at the wall of the heating sleeve was found to be 43.5°C, which is within 5°C of body temperature. Once again, this is within our safety requirement.

3 Fluid Flow & Agitation System

The fluid solution contains the live culture of a batch procedure. Fluid interactions drive critical exchanges with the live culture. Homogeneity of the fluid also determines the degree to which measurements can be deemed representative samples. Thus, a complete bioreactor design necessitates characterization of fluid flow and agitation systems.

Fluid moves through the main vessel through the use of pumps and an agitation system, where the agitation system consists of the stirring mechanisms and use of baffles. The “agitator” refers to the impeller and stirring rod, manufactured as one piece and secured to the motor via a set screw coupling.

This section describes and justifies design decisions regarding the movement of fluid through the vessel, with a focus on design of the agitation system due to complex underlying mechanics.

3.1 Determining Desired Range for Feed and Output Rates

The target range spans 0.5 to 5mL/min for feed and output rates. Based on specifications of the peristaltic pumps, our product can support 0 to 5.9mL/min with a precision of 0.1mL/min.

Typical cell replacement rates determined the target feed and output rate range in the design specification stage. Using E. coli as a model bacterium, E. coli can replicate and divide as quickly as every 20 minutes [41]. If a user aims to maintain the E. coli population at a steady state while in the stage of exponential population growth (Fig. 7) [38], the 100mL vessel volume must be replaced every 20 minutes. Feed and output rates of 5mL/min achieve this objective. In comparison, mammalian cells replace at much slower rates [40]. A rate of every 24 hours translates to steady state feed and output rates of about 0.07mL/min. Due to initial concerns about pump precision at low flow rates, the lower bound of feed and output flow control was adjusted to 0.5mL/min. However, we now expect the selected pumps to achieve adequate control at low flow rates.

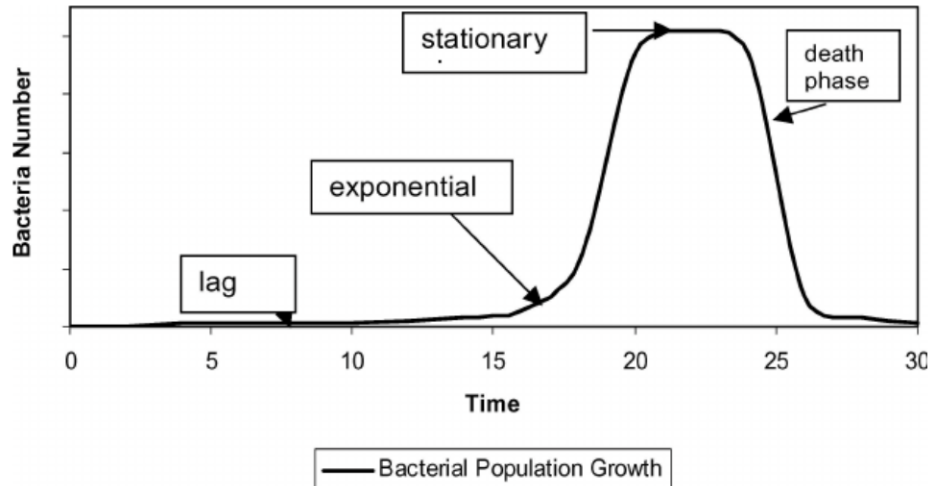


Figure 7: Population growth curve for example bacteria [38].

To set a target range specification, the feed and output rates were treated as equal. However, the feed and output rates require distinct pumps since these rates are unlikely to be equal in practice. If the feed and output volumetric flow rates matched, less liquid solution would leave than enter the vessel, as dissolved gasses would occupy some portion of the pumped volume. Thus, steady state requires modulation of the feed and/or output flow rates.

3.2 Agitation Rate Expected Range

The desired range for agitation rates spans 140 to 1000 RPM. Our product can achieve agitation rates between 0 to 1000 RPM based on motor specifications.

The expected lower bound for operational agitation rates, 140 RPM, was set by calculations considering maximum shear withstood by mammalian cells (see Appendix B), as mammalian cells are more sensitive than bacterial cells to shear force. The upper bound was initially set to 300 RPM, determined by initial findings reflecting typical bioreactor agitation rates [42, 13]. However, reaction processes may require transitive (i.e., not steady state) agitation speeds up to 1000 RPM [14].

3.3 Selection of Stirring Method

Agitation generates turbulence that facilitates mixing. Mixing increases homogeneity of the reacting solution. Turbulence is also important in facilitating the transport of scalars, such as dissolved oxygen. For this reason, agitation is a critical mechanism of bioreactors. Our product uses mechanical stirring with three 45°-pitched blades, inducing downwelling for flow through the trenches and allowing for easily exchangeable agitator mechanisms.

In laboratory settings, reacting solutions can be agitated via stirring or external vibration. Mechanical noise introduced by external vibrations would likely interfere with sensor performance. Furthermore, stirring methods are typically more easily controlled than vibrations. Consequently, most bioreactors use stirring methods for agitation.

Bioreactor designs commonly employ one of two agitation methods: magnetic versus mechanical stirring. Magnetic stirring methods utilize a rotating magnetic field to induce rotation of an impeller with magnet inserts, whereas mechanical stirring utilizes an impeller that mechanically couples to a motor. The magnetic impeller contacts the bottom face of the vessel. In contrast, the mechanically coupled impeller is best controlled from the top of the vessel, avoiding leaking risks around the stirring rod that extends outside the vessel. Mechanical stirring proved advantageous to magnetic stirring considering the limited space available on the bottom face of the vessel given the presence of sensing trenches. Furthermore, mechanical stirring impellers avoid the associated cost and complex manufacturing of impellers with magnet inserts, allowing for easily exchangeable impeller designs. Mechanical stirring methods can also be more easily modified in future iterations to enable impeller height adjustment, such that users can tune flow conditions to the reaction of interest.

Development of an impeller design (Fig. 8) focused on hydraulic efficiency, power draw, and resulting flow conditions. The design implemented 45°-pitched blades to direct flow through the trenches, thus avoiding particle accumulation that may produce unrepresentative samples. Pitched blade impellers also exhibit relatively strong hydraulic efficiency without high drag, associated with high power draw (Fig. 9) [11]. Literature review revealed that 45°-pitched impellers with one or two blades induce higher radial and axial velocities with pronounced recirculation patterns while impellers with three or four blades exhibit higher tangential velocities [2]. Designs with two or three blades perform mixing most effectively. For these reasons, a three-blade 45°-pitched impeller design was selected. The impeller diameter spans half the diameter of the vessel design to optimize energetic efficiency [10].

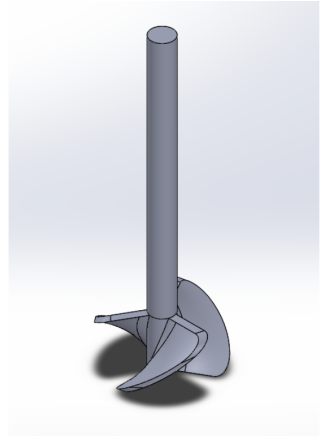


Figure 8: Combined impeller and stirring rod part for mechanical stirring, manufactured as one part. Top of the stirring rod couples to the motor shaft via a set screw. Impeller design features three 45°-pitched blades.

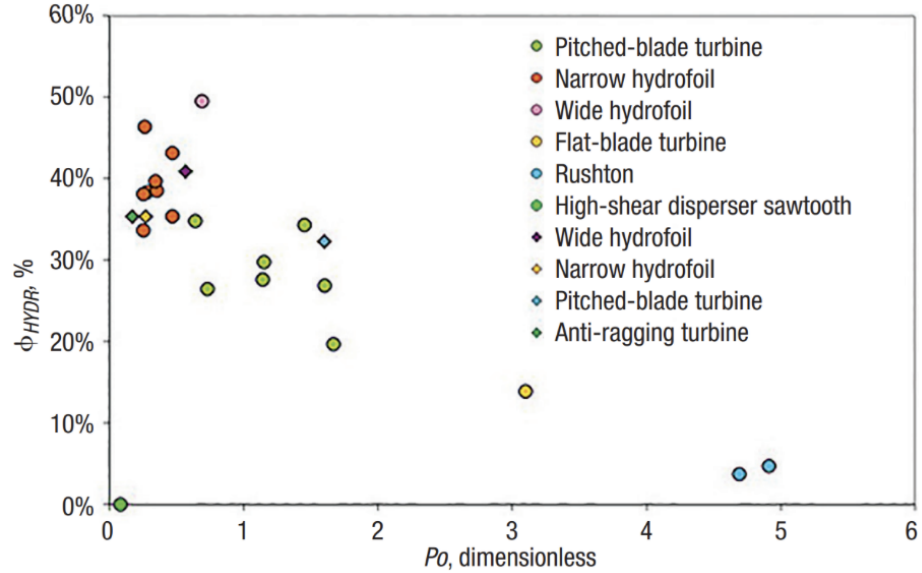


Figure 9: Hydraulic efficiency versus drag coefficient (represented by power number, Po) for various types of impeller configurations [11].

3.4 Evaluating Flow Speed in Sensing Trenches Using Fluid Simulations

Described further in Section 7.1.2, trenches on the bottom face of the main vessel allow the use of noninvasive sensing methods that require flat, parallel surfaces with a minimal intermediate gap. However, the narrow widths of the trenches raised concerns of creating stagnating flow zones within the trenches (i.e., little to no flow). Without flow in the trenches, any particle accumulation could not disperse, likely resulting in unrepresentative measurements.

To assess the main vessel design against these concerns, an incompressible fluid simulation was developed using SimScale that approximated the reacting solution with the fluid properties of water. Table 8 summarizes the simulation settings input into SimScale.

Table 8: SimScale steady-state incompressible fluid simulation settings.

SETTINGS CATEGORY	INPUT(S)
Simulation Type	Steady state
Geometry	Main vessel reacting solution ("MainVessel-water-v2")
Model	Turbulent Schmidt Number: 0.7 Diffusion Coefficients: 2e-4
Materials	Water
Initial Conditions	Gauge pressure: 0 Pa Velocity: all 0 m/s Turbulent Kinetic Energy: 3.75e-3 m ² /s ² Specific Dissipation Rate: 3.375 1/s Passive Scalar 1: 0
Boundary Conditions	All Faces but Top: wall BC, no-slip velocity, turbulence wall function Top Face: custom BC, slip velocity, zero gradient pressure, zero gradient turb. kinetic energy, zero gradient specific dissipation rate, Passive scalar value=21%
Advanced Concepts	Rotating zones: MRF rotating zone, Origin=(0,0,0), Axis=(0,0,1), Rotational velocity=[140, 200, 250, 300] RPM, Assigned volumes=(impeller + stir bar)

Under "Advanced Concepts," Table 8 lists the rotational velocities simulated in individual trials. Representing one of these trials, Fig. 10 demonstrates steady-state flow simulated with an impeller rotational speed of 300 RPM. This trial was selected for visualization for ease of identifying zones with relatively high velocity.

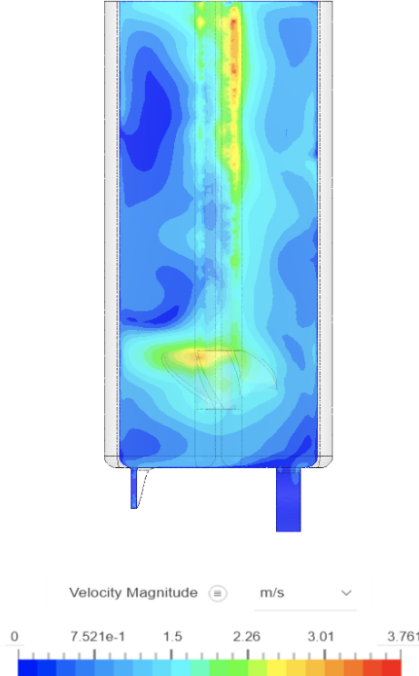


Figure 10: Steady-state incompressible fluid simulation velocity magnitude visualization across vertical midplane for an agitation rate of 300 RPM. Simulated using SimScale. Indicates low but significant flow through the trenches.

Each trial demonstrated low but significant flow through the trenches, with velocities on the order of 0.1

m/s. Figure 11 demonstrates trends revealed between trials for each trench shape. Based on these results, mechanical stirring agitation provides sufficient flow through the trenches to relieve concerns of stagnation and particle accumulation.

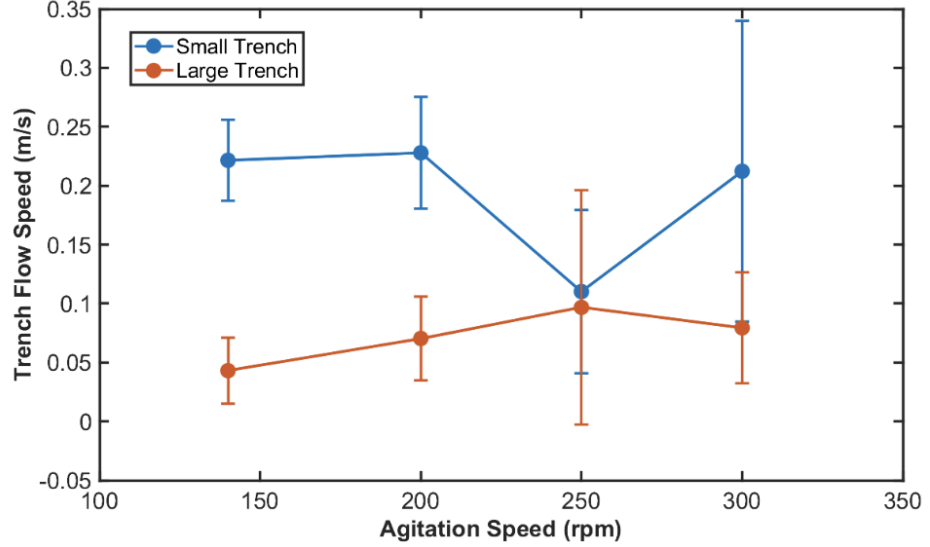


Figure 11: Mean flow speeds through sensing trenches, distinguished by relative size. Error bars represent 95% confidence intervals based on inspected points along trench centerlines.

3.5 Using Fluid Simulations to Assess Mixing

Turbulence in fluid mechanics can be quantitatively described by deviations from a time-averaged mean value (Fig. 12). Parameters can therefore be decomposed into mean u and turbulent u' parts, as denoted by Equation 11 [36].

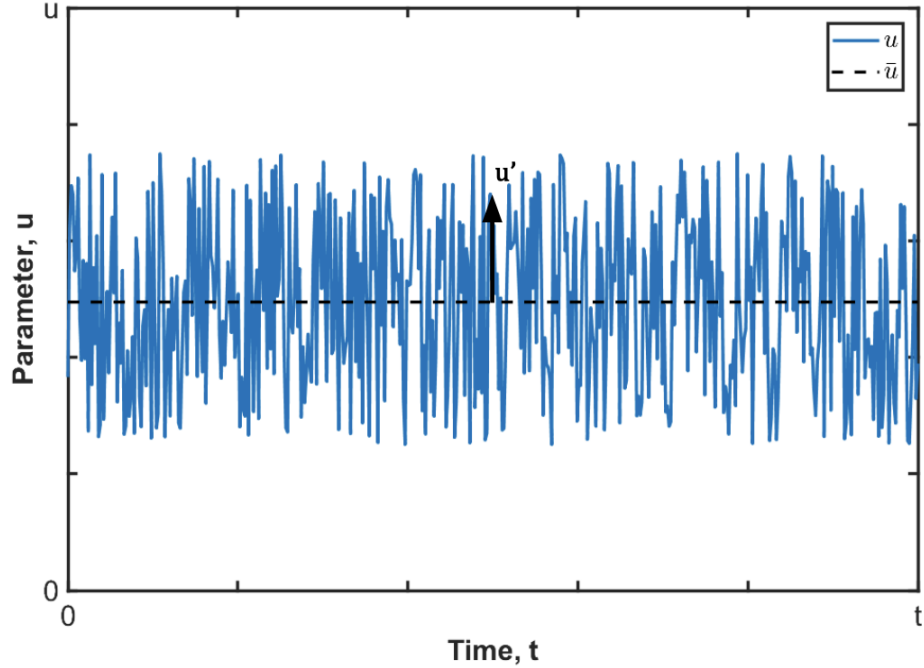


Figure 12: Time-variation for arbitrary parameter, u , visually decomposed into mean and turbulent parts, such that turbulence is represented by deviations from the dashed mean line.

$$u = \bar{u} + u' \quad (11)$$

Mixing refers to the process of combining distinct substances into a homogeneous solution. Mixing in laminar flow primarily arises from molecular diffusion, whereas eddies arising from turbulent fluctuations in turbulent flow disrupt concentration gradients. Hence, the presence of turbulence greatly enhances mixing efficiency and resulting homogeneity. For this reason, a measure of turbulence can serve as an indirect measure of mixing.

Our analysis utilized total turbulent kinetic energy (TKE) as a measure of turbulence. TKE indicates the kinetic energy per unit mass associated with turbulent fluctuations from the mean flow, defined in Equation 12:

$$TKE = \frac{1}{2}(u'^2 + v'^2 + w'^2) \quad (12)$$

where u' , v' , and w' represent turbulent velocity fluctuations in the x , y , and z directions, respectively. Total TKE summed TKE values across the vertical mid-plane of the reacting solution, evaluated for each simulation trial (Figs. 13 & 14).

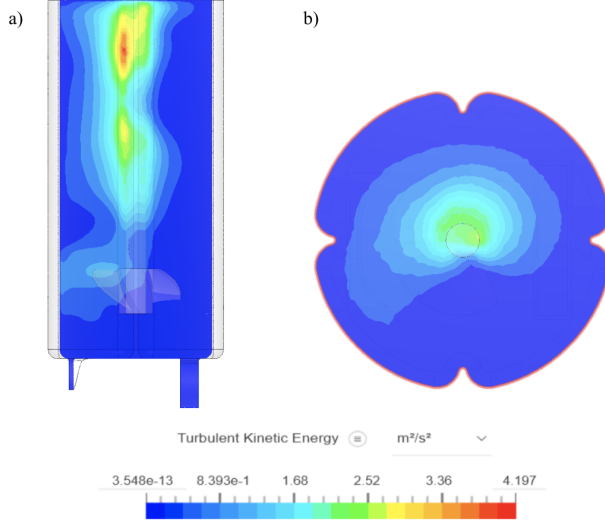


Figure 13: Steady-state incompressible fluid simulation TKE visualization across (a) vertical midplane and (b) near-top surface1 for an agitation rate of 300 RPM. Simulated using SimScale.

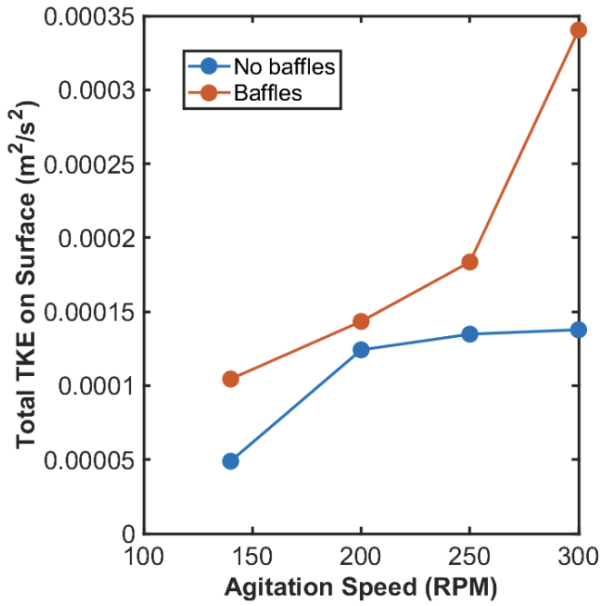


Figure 14: Total TKE evaluated as sum of TKE values across near-top surface for each agitation speed iteration in SimScale simulation.

Baffles create obstructions and consequential turbulence in the flow. Our product involves four baffles. Figure 13b depicts baffle shape and placement. Figure 14 demonstrates that total TKE across a near-top surface increases non-linearly with agitation speed and is significantly enhanced with the inclusion of baffles into the main vessel design. Using total TKE as an indirect measure of mixing, baffles effectively enhance mixing. As Fig. 14 focuses on a near-top surface, it can be stated that baffles enhance mixing at the interface between headspace gases and the reacting solution, indicating enhanced dissolved gas uptake with baffles.

3.6 Simulated Oxygen Transfer from Agitation

Use of our product for aerobic reactions requires an adequately high dissolved oxygen concentration to be dispersed throughout the reacting solution. Dissolved oxygen uptake occurs as a passive scalar transport process, where oxygen concentration is represented with a nondimensionalized scalar (fraction or percent) [12].

The SimScale fluid simulation predicted dissolved oxygen uptake at the interface between headspace gases and the reacting solution. Figure 15 demonstrates simulated oxygen transport under an agitation rate of 300 RPM as well as initial and boundary conditions described in Table 8.

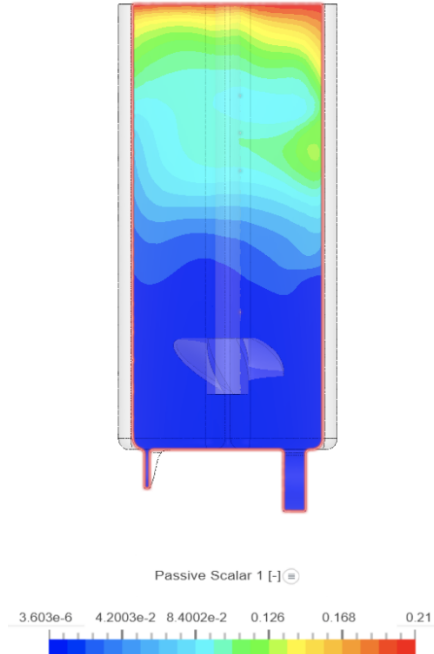


Figure 15: Steady-state oxygen concentration simulated as a passive scalar for 300 RPM agitation rate. Qualitative results indicate significant stratification and need for input gas.

The qualitative patterns depicted in Fig. 15 for 300 RPM agitation represent steady-state oxygen concentration patterns observed for each trial of the simulation. The visually stratified results indicate that a reliance only on transport at the headspace-solution interface leads to poorly distributed oxygen concentrations. Thus, the simulation results justify the use of gas input tubes, particularly for crucial oxygen uptake.

4 Sensors

The bioreactor's sensing system consists of four sensor packages: 1) temperature, 2) pH, 3) dissolved oxygen (DO), and 4) optical density (OD). The temperature, pH, and DO sensors and their control systems are critical to maintaining the proper environment within the bioreactor to enable healthy bacterial and cell growth and maximize product yield. Compromising these parameters can significantly impact growth rate, product formation, and cell viability. The OD sensor is used to measure the growth rate of the culture. This is necessary to identify and monitor the growth phase of the culture, which influences several other reaction parameters, such as feed rate, product yield, and reaction efficiency.

The sensing system is entirely non-invasive to eliminate the need to sterilize or replace the sensors after every use and to minimize the risk of contamination to the broth that comes with introducing additional components into the reaction chamber. By decoupling the sensors from the disposable vessel, the bioreactor is easily serviceable, as individual components can be replaced without affecting the rest of the system.

4.1 Temperature Sensor

Requirement: $25-50 \pm 0.5^{\circ}\text{C}$

4.1.1 Temperature Sensor Working Principle

The bioreactor requires temperature measurement for optimizing the reaction environment within the vessel. The thermal sensing system measurement requirement was determined to be $25-50 \pm 0.5^{\circ}\text{C}$ in 30 seconds as determined by the sponsor's functional requirements. A key goal in designing the sensing system was also to maintain non-invasive sensing. This requires the temperature sensor to be located on the outside of the vessel. Because the heating system is placed on the side of the vessel to maximize heated surface area, the temperature sensor is located on the bottom of the vessel (Figure 16).

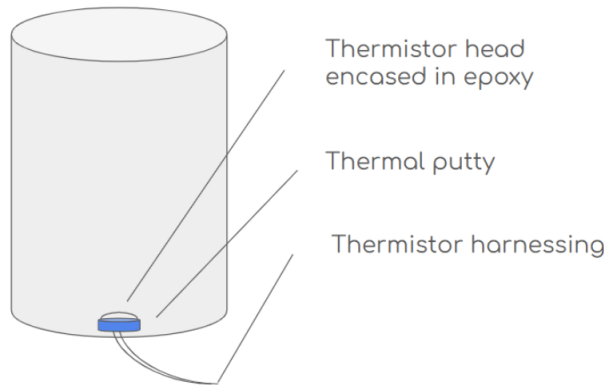


Figure 16: External Thermistor Placement Diagram

This is a well insulated location in the middle of the device that can be well characterized with a 1-Degree representation of the thermal characteristics. This estimation is outlined in section 2.5, which determines a time constant of 20 seconds, which is within the requirement of 30 seconds. Based on these considerations, we selected thermistors from the NRCE family as our sensing method. There are several advantages to the use of thermistors in the application of bioreactors:

- 1. Non Invasive Measurement:** The thermistor does not directly contact the interior of the bioreactor, which maintains sterility. This implementation is common in the design of high voltage battery pack systems, where temperature sensing methods are required to be isolated from the point of measurement.
- 2. High Sensitivity:** The chosen thermistor can detect minute temperature changes using the provided temperature data which can be mapped and linearized to any resistance value.

3. **Cost Effectiveness:** Thermistors are inexpensive and easy to implement in software, which make them ideal for large scale production. The chosen thermistor costs about \$0.10 when ordered in bulk quantities.
4. **Compact Size:** Compact size allows for easy packaging into the bioreactor geometry. The NRCE family of thermistors feature a diameter of only 6.5mm.
5. **Fast Response Time:** Thermistors respond quickly to temperature changes, which enables real time temperature monitoring. Thermistors from the NRCE family feature a temperature sensing time constant of about 20 seconds.

These key features allow for reliable and low cost implementation of temperature sensing.

4.1.2 Temperature Sensor Circuit Design Considerations

NTC thermistors provide excellent temperature sensing capabilities and high sensitivity. The characteristic curve is typically non-linear and can be measured using an embedded circuit that will allow a corresponding voltage to be measured. However, direct resistance measurements present challenges in accurate reading which stems from internal resistances of measurement devices and voltage drops across leads and connectors. A null comparator can be used to avoid such issues.

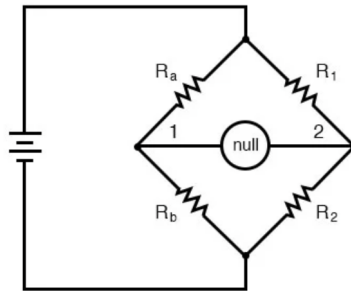


Figure 17: Wheatstone Bridge Circuit (Null Comparator)

Figure 17 shows a Wheatstone Bridge circuit, also known as a null comparator. This circuit is widely used due to its simplicity and reliability in obtaining precise resistance measurements. It can be used to measure unknown resistances accurately to calibrate sensors. It operates on the principle of voltage dividers and achieves balance when the ratios of resistance across both sides are equal. Branch 1 has two known resistors, and branch 2 has a known resistor and an unknown resistor. A null detector is connected between the two branches. The null detector measures the voltage difference between the midpoints of the two branches. When the bridge is unbalanced, a voltage will be measurable across the null detector. One of the resistors is a variable resistor, which will be adjusted until the null detector reads zero. At this stage, the wheatstone bridge is in a balanced state, and can be represented by the following expression:

$$\frac{R_1}{R_2} = \frac{R_3}{R_X} \quad (13)$$

The above expression can be solved to find the unknown resistance.

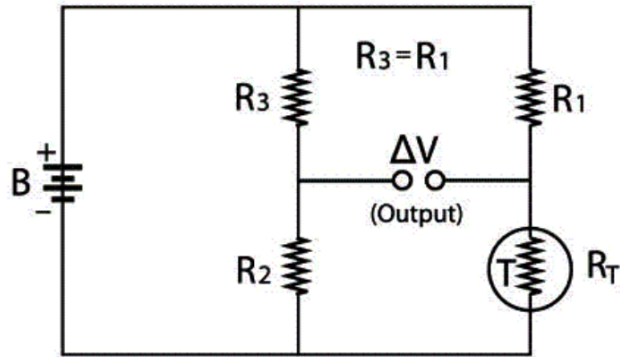


Figure 18: Thermistor (R_T) Measurement Circuit

The circuit can be modified as shown above in Figure 18, where the unknown resistor has been replaced with a thermistor. This method of measuring thermistor resistance has a number of advantages:

1. **Low power consumption:** Because the sensor relies on reaching a state of no current flow, the power consumption required for operation is greatly reduced.
2. **Not sensitive to supply voltage fluctuation:** the balance does not depend on supply voltage, only resistance ratios which do not affect the calculation of resistance.
3. **Accuracy:** Effects of series resistance inaccuracies are reduced greatly.

4.2 pH Sensor

Requirement: 4-9 pH

4.2.1 pH Sensor Working Principle

To measure the pH of the reaction, our product uses a polyaniline (PANI) sensing layer, which changes its absorbance based on the pH that it is exposed to. A plot of the absorbance versus wavelength is shown in Figure 19.

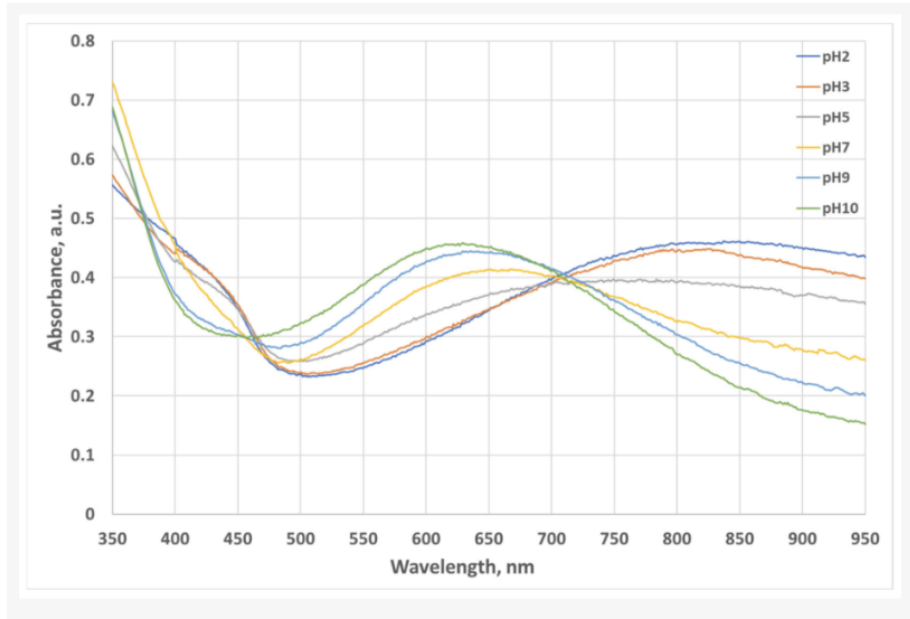


Figure 19: Absorbance spectrum of $8\mu\text{m}$ thick PANI film [35].

4.2.2 NIMBLE's pH Sensor

To observe this effect, we shine light using an LED at $\sim 630\text{nm}$ and we observe the intensity of light that makes it through the PANI layer using a photodiode. A very similar method has been demonstrated to work [35]. In that work, the authors deposited the PANI film directly on the LED and photodiode and submerged them in solution, as shown in Figure 20.

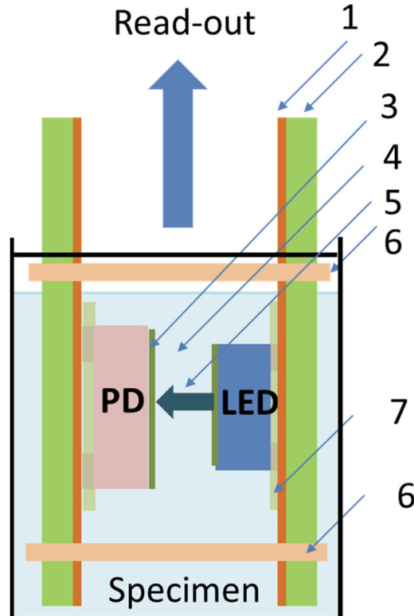


Figure 20: Fundamental diagram of the pH sensor demonstrated by researchers at the University of Liege in Belgium. They deposit the PANI layer directly onto the photodiode and LED and submerge the whole system in solution.

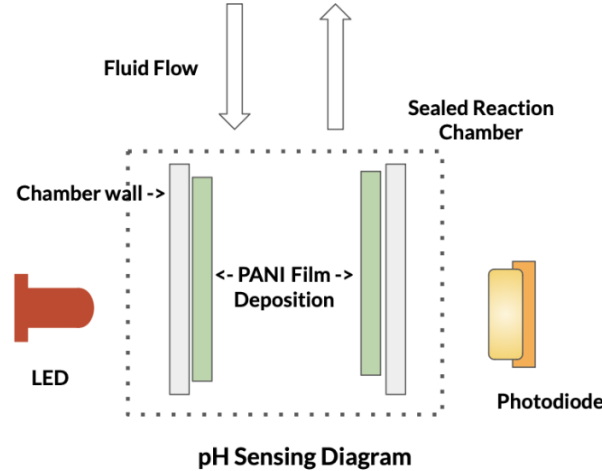


Figure 21: Fundamental diagram of the NIMBLE pH sensor.

For our application, we placed the LED and photodiode across a “trench” in the bottom plate of the chamber, we deposited the PANI film on the inside of the chamber, and we added a reference photodiode to help account for LED intensity variation over time.

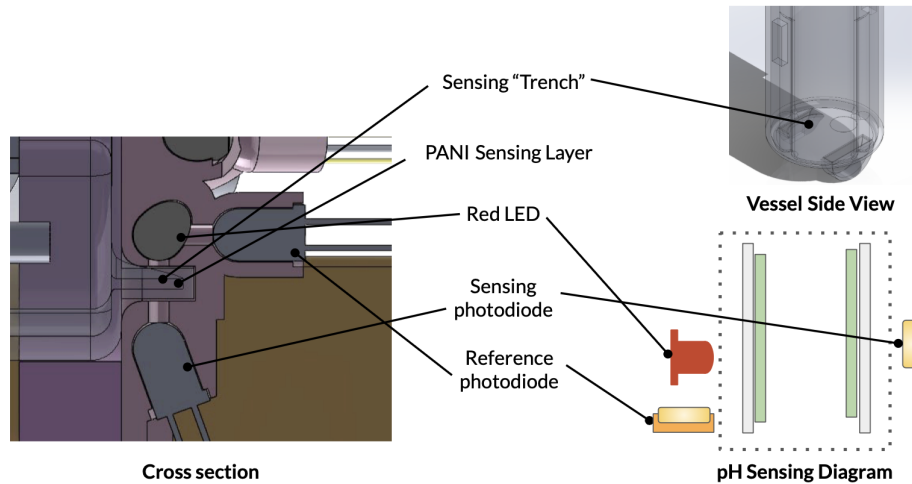


Figure 22: Packaging diagram of the pH sensor.

4.2.3 pH Amplifier Circuits

We will need amplifier circuits for both the sensing and reference photodiodes in the pH sensor. To design these circuits, we first need to estimate the signal on the photodiodes. Start with the sensing photodiode.

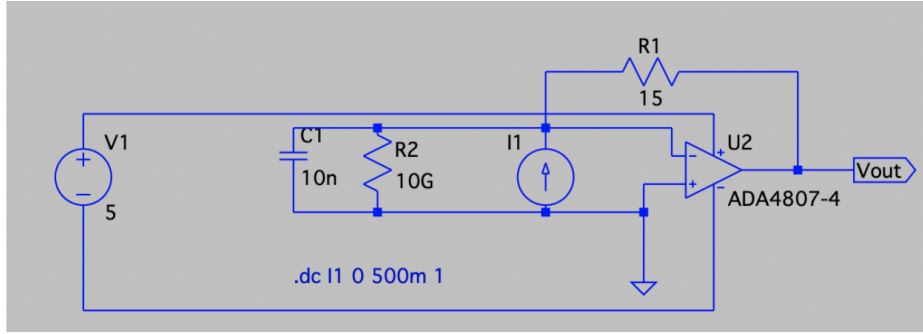


Figure 23: Sensing circuit for pH sensing photodiode. We expect 0.131mA of max current, so according to equation 16 (described in the dissolved oxygen analysis), we choose $R_1 < 38 \text{ k}\Omega$.

We designed a circuit for the sensing photodiode (see Figure 23), starting with an estimate of current generated. We expect to generate $\sim 0.131\text{mA}$ of current in the sensing photodiode at peak signal (with pure water). This was calculated as follows:

$$8\text{mW} \times \frac{6}{4\pi \times (3\text{mm})^2} \times 0.5 \times 1\text{mm}^2 \times 0.62 \frac{\text{A}}{\text{W}} = 0.131\text{mA} \quad (14)$$

Equation 14 was derived from the following process model:

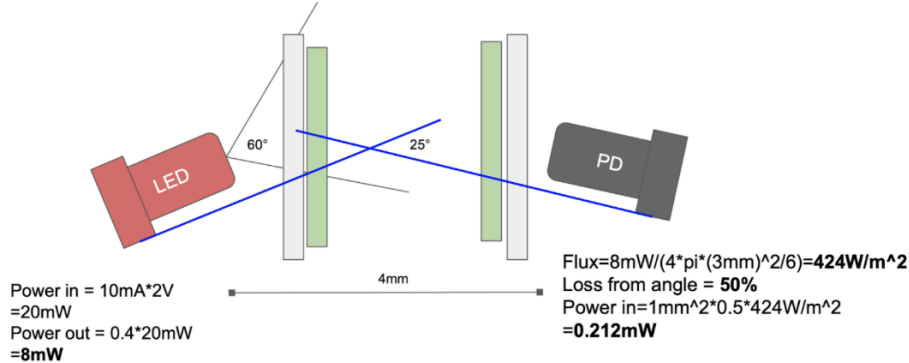


Figure 24: Simplified geometry diagram of pH photodiode and LED.

1. 8mW was calculated to be emitted from the LED based on the manufacturer specification for BOM Part 1.
2. 424 W/m² was calculated to be incident on the photodiode based on a distance of 4mm and 60° viewing angle, using the Flux calculation for a spherical source, as described by Figure 25.

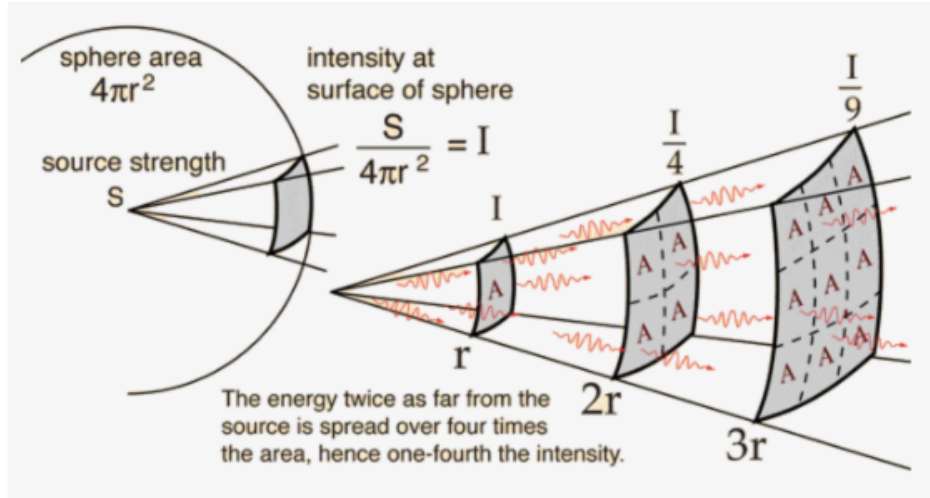


Figure 25: Flux calculation from spherical source [34].

3. There is a 50% loss based on a 25° angle. The manufacturer does not specify the spatial radiation distribution, so this is estimated based on other LEDs and PDs.
4. There is a 1mm² active area for the photodiode, as specified by the manufacturer for BOM Part 2.
5. 0.62 A/W photodiode responsivity at 600nm based on the manufacturer specification for BOM Part 2. A plot of this responsivity is shown in Figure 26.

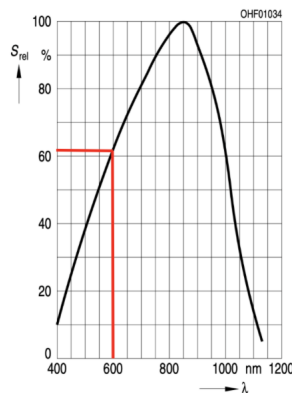


Figure 26: Current generated per watt of incident light, vs wavelength

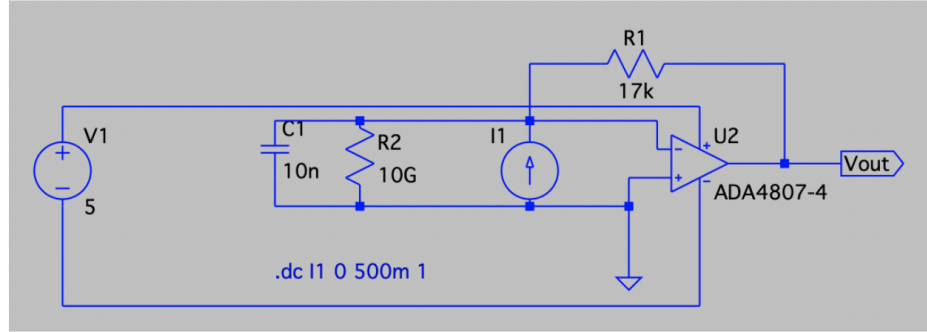


Figure 27: Sensing circuit for pH reference photodiode. We expect 0.248mA of max current, so according to equation 16 (described in the dissolved oxygen analysis), we choose $R_1 < 20.1 \text{ k}\Omega$.

We also designed a circuit for the reference photodiode (see Figure 27), starting with an estimate of current generated. We expect to generate $\sim 0.248 \text{ mA}$ of current on the sensing photodiode. This was calculated as follows:

$$8\text{mW} \times 0.05 \times 0.62 \frac{\text{A}}{\text{W}} = 0.248\text{mA} \quad (15)$$

Equation 15 was derived from the following process model:

1. 8mW was calculated to be emitted from the LED based on the manufacturer specification for BOM Part 1.
2. 5% of this will be incident on the reference photodiode, as estimated from the geometry.
3. 0.62 A/W photodiode responsivity at 600nm based on the manufacturer specification for BOM Part 2.

4.3 Dissolved Oxygen Sensor

Requirement: 2-9 mg/L

4.3.1 Dissolved Oxygen Working Principle

To measure the dissolved oxygen (DO) of the reaction, our product uses a sensing layer made of a Tris (4,7-diphenyl-1, 10-phenanthroline) ruthenium(II) Complex in Sol-Gel, which changes fluorescence based on the dissolved oxygen concentration it is exposed to. Fluorescence is the material property of “visible or invisible radiation emitted by certain substances as a result of incident radiation of a shorter wavelength such as X-rays or ultraviolet light” [7].

As the dissolved oxygen concentration increases in contact with the Ru-complex layer, the fluorescent intensity is quenched, and so the emitted light is decreased. Experimental results show this relationship:

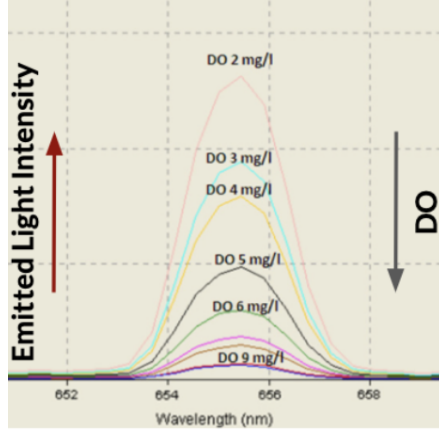


Figure 28: Fluorescent spectrum of the Ru-complex layer with changing dissolved oxygen concentrations [1]

This relationship is described well using the Stern-Volmer equation:

$$\frac{I_0}{I} = 1 + K_{sv} \times [Q], \quad (16)$$

where I is the measured fluorescence intensity with quencher concentration $[Q]$ present, I_0 is the measured fluorescence intensity without quencher present, and K_{sv} is the Stern-Volmer constant.

4.3.2 NIMBLE's Dissolved Oxygen Sensor

We will use this working principle to create our dissolved oxygen sensor in a very similar way as previously demonstrated in the literature [1]. An overall schematic is shown below:

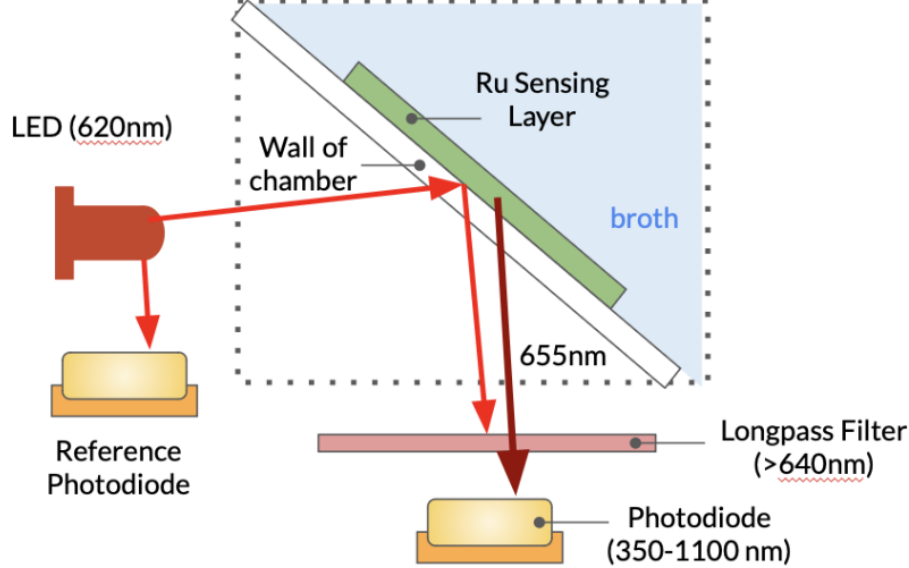


Figure 29: Dissolved oxygen sensor diagram.

We shine light using an LED at 620nm on the Ru-complex layer, generating the fluorescence effect and therefore causing emission of our signal at 655nm. This signal is detected using a photodiode, which is placed

behind a 640nm longpass filter. This longpass filter blocks the light from the LED, so that the photodiode only reads the signal. We also add a reference photodiode to help account for LED intensity variation over time.

For our application, we place the sensing layer in a small circular recession in the bottom of the chamber. We mount the LED and photodiode such that they are facing the layer.

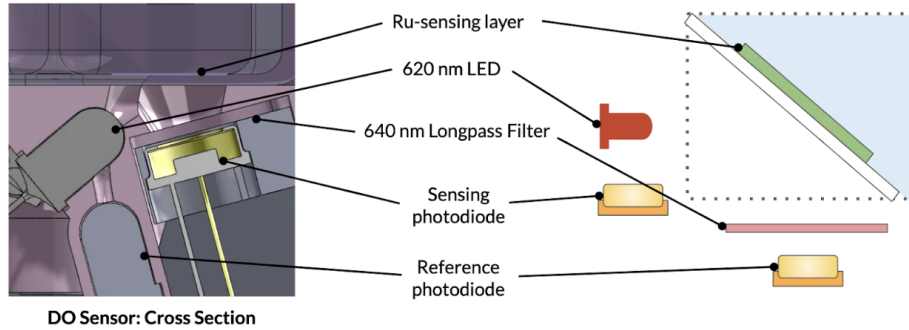


Figure 30: Packaging diagram of the dissolved oxygen sensor.

4.3.3 DO Amplifier Circuits

For this expected current, we designed an amplifier circuit. This circuit has 2 functions:

1. Convert the current signal from the photodiode into a voltage signal we can feed into the Raspberry Pi (via an ADC, see section 5.3).
2. Amplify the voltage signal so that it is easily detectable.

First, we find the max current we expect to see. We expect to generate $\sim 0.5\text{mA}$ of current in the sensing photodiode with no oxygen (peak signal). This was calculated as follows:

$$9\text{mW} \times 0.8 \times 0.5 \times 0.5 \times 0.8 \times 0.35 \frac{A}{W} = 0.504\text{mA} \quad (17)$$

Equation 17 was derived from the following process model:

1. 9mW is emitted from the LED based on the manufacturer specification from BOM Part 6.
2. 80% of this light is incident on the fluorescent layer, as estimated based on geometry and calculated according to Figure 31.

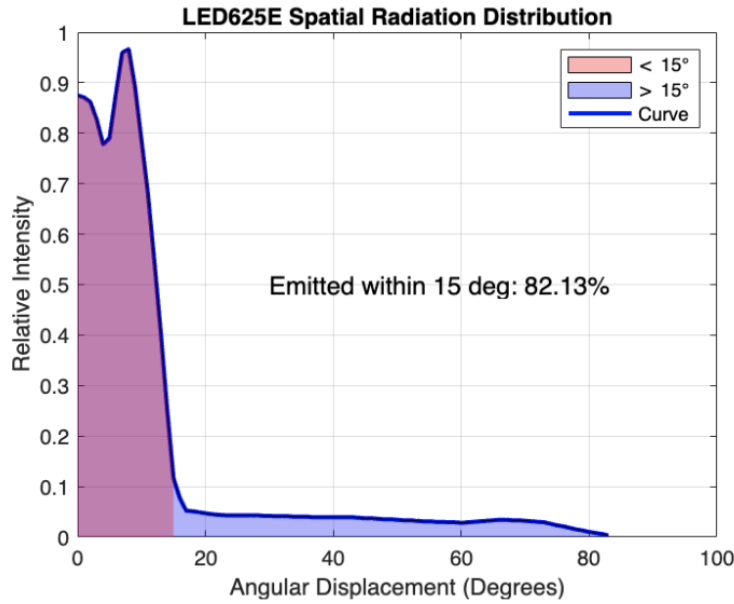


Figure 31: Recreated curve from datasheet, integrated from 0-15 degrees using Matlab. This script is provided in Appendix C. This could be modified to calculate radial distribution for other photodiodes and LEDs.

3. 50% of this light will be reemitted from the fluorescent layer at 655nm, as estimated based on vibes.
4. 50% of this re-emitted light will be incident on the filter, as estimated based on geometry.
5. 80% of 655nm light will pass through the filter base on manufacturer specification from BOM Part 7. The transmittance spectrum is shown in Figure 32.

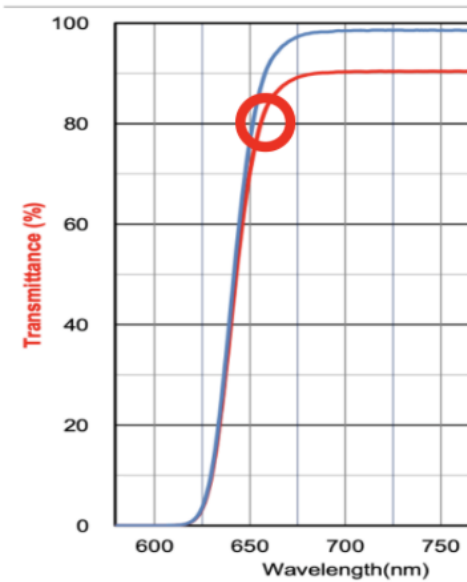


Figure 32: Filter transmittance vs wavelength.

6. 0.35 A/W photodiode responsivity at 655nm based on manufacturer specification from BOM Part 8.

This responsivity plot is shown in Figure 33.

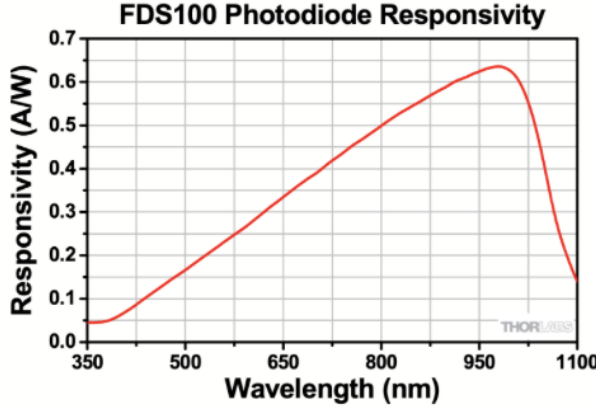


Figure 33: Current generated per watt of incident light, vs wavelength.

The transimpedance circuit has the following characteristic equation [28]:

$$V_{out} = -I_1 \times R_1 \quad (18)$$

For this purpose, we designed a transimpedance circuit utilizing an op amp ADA4807-4, a 9.2k Ohm resistor, 1nF unpolarized metal-film capacitor. The photodiode equivalent circuit we used for this model was derived from the datasheet for part 8. The schematic is shown below:

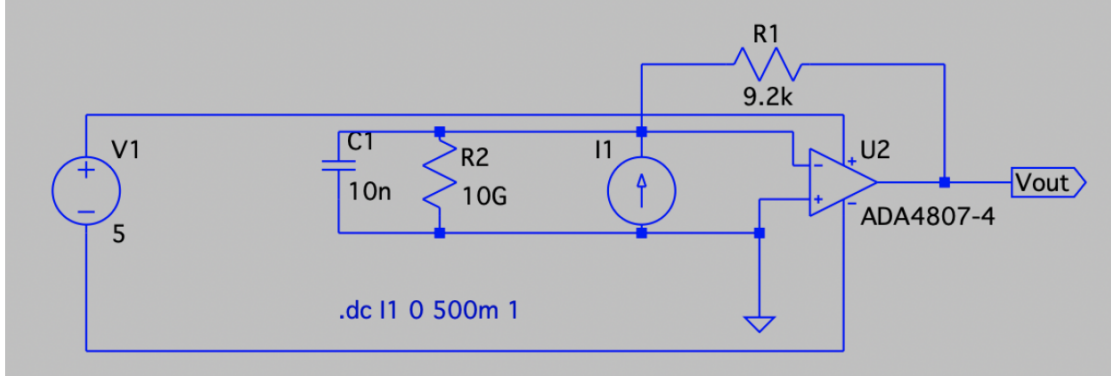


Figure 34: Sensing circuit for dissolved oxygen sensing photodiode.

We also designed a circuit for the reference photodiode (see Figure 36), starting with an estimate of current generated. We expect to generate ~ 0.293 mA of current on the sensing photodiode. This was calculated as follows:

$$9\text{mW} \times 0.05 \times 0.65 \frac{\text{A}}{\text{W}} = 0.293\text{mA} \quad (19)$$

Equation D was derived from the following process model:

1. 9mW is emitted from the LED based on manufacturer specification for BOM Part 6.
 2. 5% of this light is incident on the reference photodiode layer, estimated based on geometry.
 3. 0.65 A/W photodiode responsivity at 620nm based on manufacturer specification for BOM Part 8.
- This responsitivity plot is reproduced below in Figure 35.

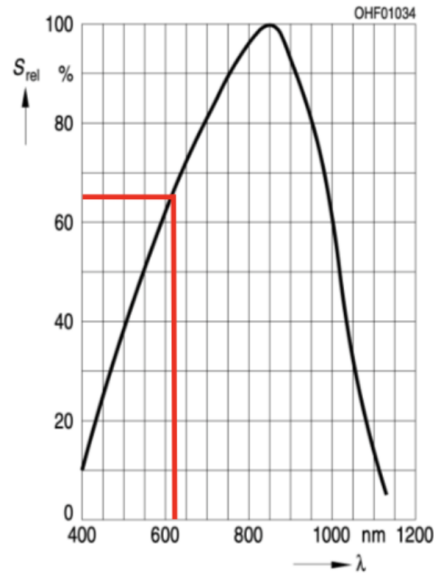


Figure 35: Current generated per watt of incident light, vs wavelength.

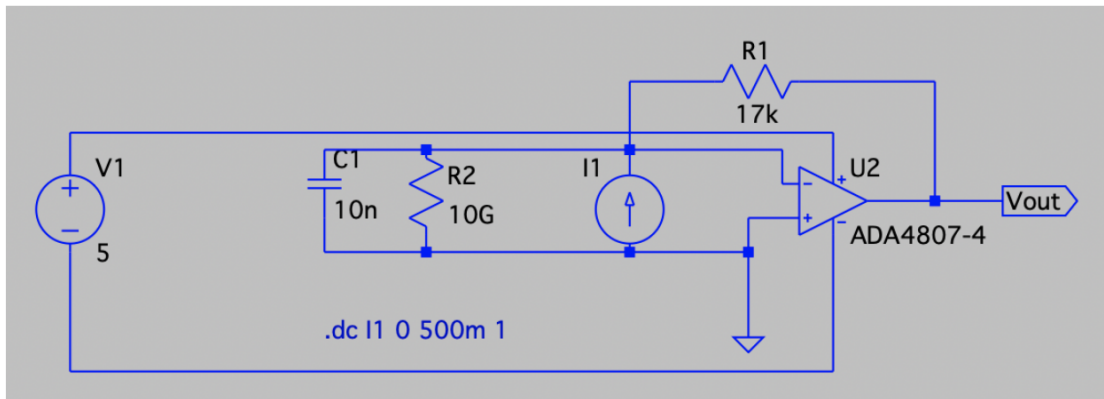


Figure 36: Sensing Circuit for dissolved oxygen reference photodiode. We expect 0.293mA of max current, so according to Equation 19, we choose $R_1 < 17 \text{ k}\Omega$.

Using this setup, we expect to recreate the linear relationship as demonstrated in the literature:

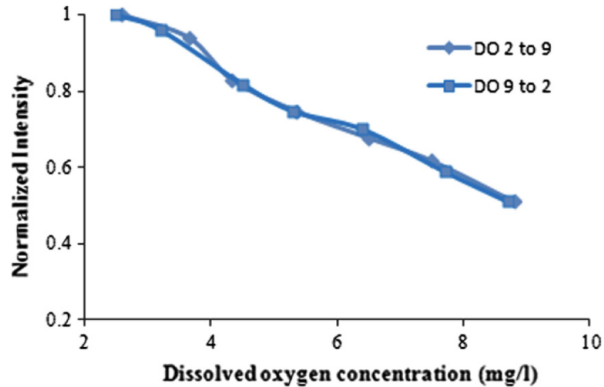


Figure 37: Detected intensity vs dissolved oxygen concentration using the Ru-complex layer. This shows negligible hysteresis [5].

4.4 Optical Density Sensor

Requirement: $0\text{-}2 \pm 0.1\text{au}$

4.4.1 OD Working Principle

Optical density (OD) is based on the linear relationship between light absorbance and particle concentration. To measure the OD of the reaction, our product uses an LED, a reference photodiode, and two measurement photodiodes. Light is emitted from the LED and is scattered by the suspended particles in the culture. Some of this scattered light is detected by a photodiode, which measures its incident intensity. As the culture grows, the optical density increases and results in a greater intensity of light being detected by the photodiode due to increased scatter.

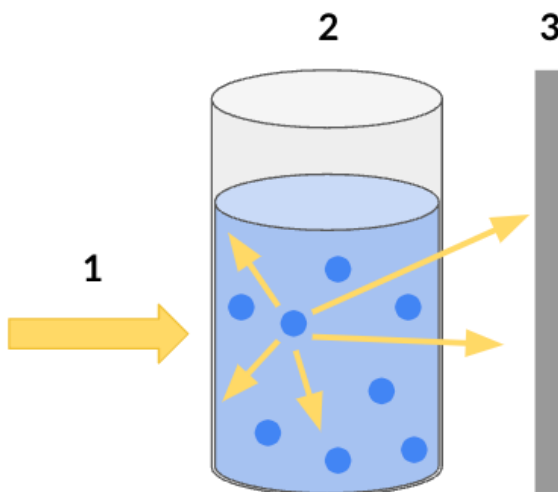


Figure 38: Light is emitted from a light source toward a cuvette of homogeneous solution, where it scatters upon collision with the suspended particles. A detector on the other side measures the intensity of scattered light that hits it.

This relationship is described by the Lambert-Beer Law:

$$A = \log \left(\frac{I_0}{I} \right) = \varepsilon cl \quad (20)$$

The Lambert-Beer Law empirically relates the attenuation in intensity of a beam passing through a macroscopically homogeneous medium. A is the absorbance, ε is the molar absorption coefficient, c is the molar concentration, and l is the optical path length [33].

Hence, rather than directly measuring the density of cells in the medium, the OD sensor measures the turbidity of the solution. Turbidity is the measure of how cloudy a solution is due to the concentration of particles it contains.

4.4.2 NIMBLE's OD Sensor

We emit light at 600 nm from the LED, the most common wavelength used in OD sensors for bioreactors. This is because 600 nm is not harmful to most bacterial cultures, unlike shorter wavelengths, and has a good balance between light absorption and scattering such that additional scattering due to other pigments in the solution is minimized [32].

For our application, we place the LED and three photodiodes around a circular trench at the base of the vessel, as shown in Figure 39. This allows us to measure a representative sample of the broth in the system rather than using the conventional method of taking samples out of the vessel for analysis. The LEDs and photodiodes are enclosed within a sensor mount to ensure that extraneous light, such as ambient or that from neighboring LEDs, does not enter the photodiodes and affect the measurements.

LED intensity will gradually dim over time and can be significantly affected by changes in temperature. Since the vessel can be heated from 25 to 50°C, depending on the reaction, it is important to account for these fluctuations by directly measuring the LED's intensity via a reference photodiode. This value is used as the emitted intensity, I_0 , used in Equation 20.

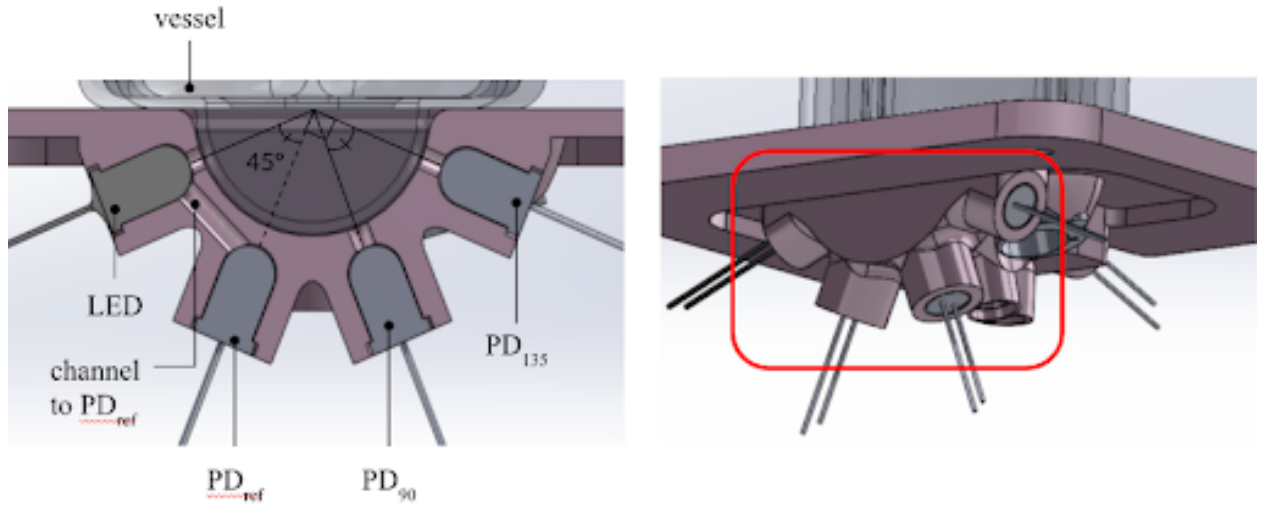


Figure 39: Packaging diagram of OD sensor. A channel runs directly from the LED to the reference photodiode to ensure an accurate reference measurement of the LED's emitted intensity.

Each sensor component is placed 45° apart from its neighbor such that there is a reference photodiode at 45° and two measurement photodiodes at 90° and 135° from the LED, respectively. A very similar packaging of the LED and photodiodes has been implemented in the Pioreactor [23]. In that device, the sensor components are arranged around the circumference of the main vessel body itself. However, due to the larger vessel diameter of our product—4cm for our product versus about 2cm for the Pioreactor—it would be difficult to achieve the desired OD sensitivity. Therefore, to better package the OD sensor and

respect the specifications of off-the-shelf LEDs and photodiodes, we mimicked a similar geometry by using a round trench.

Similar to the Pioreactor, our product has photodiodes at two different angles, 90° and 135°. At low optical density, the photodiode is more sensitive to the incident light and saturates quicker at larger angles, whereas at high optical density it saturates quicker at smaller angles. Additionally, OD has a finite regime for which the LEDs and photodiodes maintain a linear relationship. Beyond this point, OD readings become difficult to correlate [26]. Depending on the culture and LED properties, the photodiodes at different angles may have different levels of linearity. It is important to test and configure this before beginning the reaction to determine which photodiode to use.

4.4.3 OD Analysis

The reported OD value depends on several factors, such as beam intensity, photodiode spec design, and culture media, and may vary significantly between similar samples. Therefore, it cannot be taken as an absolute value and should be normalized to enable meaningful comparison.

To normalize the raw OD measurement, a reference value must first be determined by averaging a series of initial OD readings using the same solution. Then, the normalized OD can be found by dividing the raw OD by the reference, as follows:

$$\text{normalized OD} = \frac{\text{latest OD}}{\text{reference OD}} \quad (21)$$

The normalized OD represents the rate of culture growth. Thus, if normalized OD is 1.5, this implies that the culture has grown 1.5 times since the state at which the reference OD measurement was taken.

To further improve the accuracy of the OD measurement, the blanked normalized OD can be used [24]. Blanking involves measuring the OD of the media without the culture (i.e. bacteria, cells, or other microorganisms). This allows OD to be calibrated to the reaction by accounting for any turbidity contributed by the media itself. It is recommended to use this for reactions that begin with a low OD. The blanked normalized OD can be calculated using the following equation:

$$\text{blanked normalized OD} = \frac{\text{latest OD} - \text{blank OD}}{\text{reference OD} - \text{blank OD}} \quad (22)$$

Once OD has been normalized, it needs to be correlated to culture growth rate. The implied growth rate is the rate of change of the size of the culture normalized by the size of the culture:

$$gr(t) = \frac{n\text{OD}'(t)}{n\text{OD}(t)} \quad (23)$$

Although this does not give the exact cell density of the culture in terms of cell/mL, plots of the change in OD over time and the implied growth rate (see Figure 40) can give the same information regarding culture growth phase and, thus, the overall health of the culture. During the lag phase, there is no observed growth, but there is a high cell density as this is when the cells are in a nutrient rich environment and are preparing for growth. As such, the nOD(t) plot would show a near zero slope and the gr(t) plot would appear fairly stable. In the exponential phase, cells are dividing and doubling in quantity. Thus, nOD(t) shows an exponentially increasing OD, while gr(t) has a positive slope. The stationary phase is when culture growth reaches a plateau as the nutrients get used up. Since the number of dividing cells approaches the number of dying cells, nOD(t) becomes constant and gr(t) drops to zero.

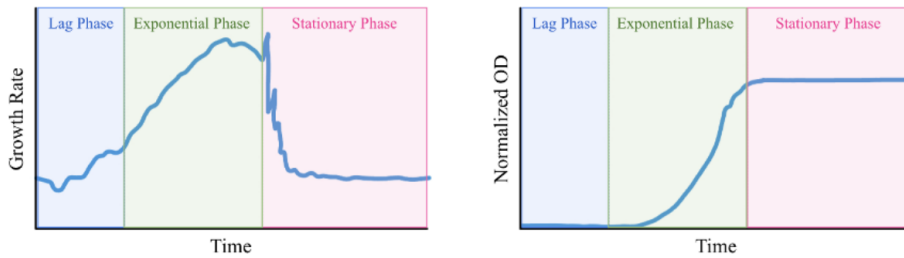


Figure 40: Culture growth phases can be identified via $nOD(t)$ and $gr(t)$ plots to monitor the health of the culture and adjust parameters such as feed rate and output rate or know when to end the reaction and prepare a new batch.

To obtain an exact correlation between OD and cell density, the conventional method of measuring samples of various density must be used to determine the empirical standard curve. This procedure can be done with our product but is not a built-in function as this must be done manually.

4.4.4 OD Amplifier Circuits

We will need individual amplifying circuits for each of the three photodiodes used in the OD sensor. We do not know how much light will get scattered and therefore how much light is incident on the photodiodes. We will have to test this device before we can design optimal circuits to amplify its signal.

4.5 Sensors Calibration

Before running an experiment, our bioreactor's sensors must be calibrated to ensure accurate results. For all sensors, we outline a 1-point calibration procedure. However, we anticipate the calibration to be dependent on manufacturing uniformity of the sensors and the customer's requirements. Thus, 2-point calibration procedures may be necessary. This would involve adding solutions of known DO, OD, temperature, and pH and collecting another data point for reference. Literature on our sensing methods, suggest that 1-point calibration should be sufficient. To perform 1-point calibration for each sensors, the following procedure should be followed:

1. Remove a new sterilized vessel from its packaging
2. Calibrate the DO sensor
 - (a) Add 10mL of deionized water
 - (b) Leave the lid partially covered for 10 minutes
 - (c) Enter the current altitude into the user interface. NIMBLE will take a temperature reading and using these values, calculate the expected equilibrium oxygen.
 - (d) NIMBLE will use the photodiode current and expected dissolved oxygen concentration to create the offset for the equation:
 - i. Note: m must be determined from DO layer testing with the final synthesis method.

$$I_{PD} = \text{Offset} - m[\text{DO}] \quad (24)$$

3. Calibrate the pH sensor
 - (a) Fill the vessel with acid or base to create a solution of known pH
 - i. Note: solution must be between 5-9 pH, or there is a risk of sensor damage.
 - (b) NIMBLE will use the current reading and known pH value to determine the offset current via the relationship

- i. Note: A, B, and C must be determined from PANI layer testing with the final synthesis method.

$$I_{PD} = \text{Offset} + \frac{A}{1 + \exp(B(pH - C))} \quad (25)$$

(c) The offset current will determine the Current vs. pH curve, as shown in Figure 41.

4. Pour out the solution

5. Fill the vessel with the starting medium for the reaction

6. Calibrate the OD sensor

- (a) Take 3 measurements of the initial OD value and average these to determine the reference OD.
- (b) Use the normalized or blanked normalized OD equation, Eq. 21 or 22, respectively, as described in Section 4.4.3 OD Analysis.

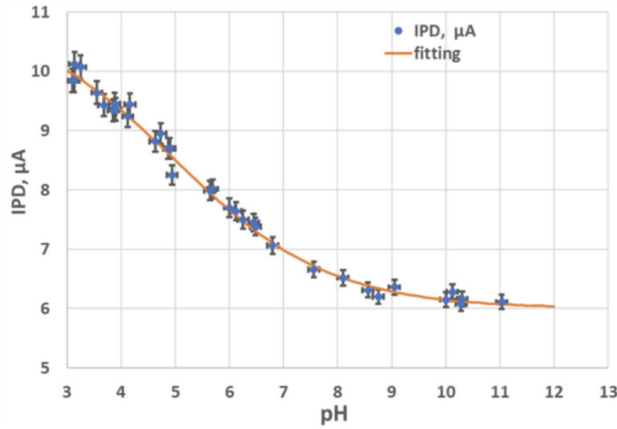


Figure 41: The current vs. pH curve is used to determine the offset current based on a known pH in order to calibrate the pH sensor. The relationship of this curve is described by Equation 25 [35].

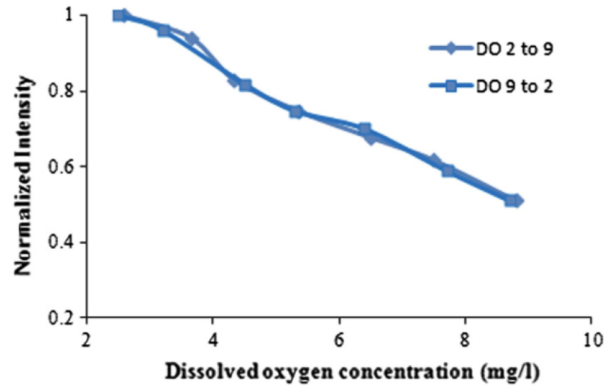


Figure 42: The normalized intensity vs. DO concentration curve is used to correlate the current signal reported by the DO sensor to a DO concentration value [5].

4.6 Sensors Testing

With extra time during 2.013 in the Fall of 2024, we spent some time testing and developing the fabrication methods for the sensors. While the working principles behind all of the sensing methods have been demonstrated in other products or in literature, we altered them slightly to incorporate in our bioreactor design. While we believe these alterations will work (see Sections 4.1-4.4), it is important to verify this.

We focused this testing on the pH polyaniline (PANI) layer. While we have an initial testing procedure for the dissolved oxygen (DO) ruthenium layer, we did not have time to receive the necessary hardware to test this, as this sensing method was added later in the semester.

4.6.1 pH Polyaniline (PANI) Layer

To determine the feasibility of the PANI layer for pH sensing and benchmark our sensor setup to a similar method that has been demonstrated to work in a paper by Serguei Stoukatch et al. [35], we needed to replicate the PANI layer in lab.

The testing procedures that we used were developed based on the procedures followed in Stoukatch's paper as well as that of the Prasad Lab [27]. Stoukatch's method used a heated environment and short deposition time, whereas the Prasad Lab used a cooled environment and long deposition time.

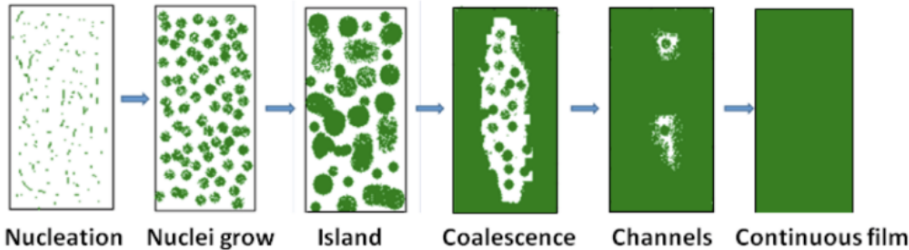


Figure 43: Nucleation stages of polyaniline as it develops into a uniform layer on a surface [17].

As the PANI layer develops, it goes through several stages of growth, starting from nucleation to forming islands to coalescence of these islands to a continuous film, as shown in Figure 43. To model the PANI layer deposition, we use the stagnant film model for growth involving a reaction. This process is well described by Figure 44.

To create the film aniline monomers must diffuse to the surface and polymerize. The polymerization reaction is a thermally activated process, whereas the diffusion has a weaker dependence on temperature. Therefore, by actively cooling the reaction like the researchers from the Prasad Lab, we can force the process into the reaction-rate limited regime (see Figure 45). This makes the reaction rate independent of the mass transport rates (i.e. there is an abundance of reactants at the surface, and the surface reaction rate is slow). This increases the uniformity of the deposited film.

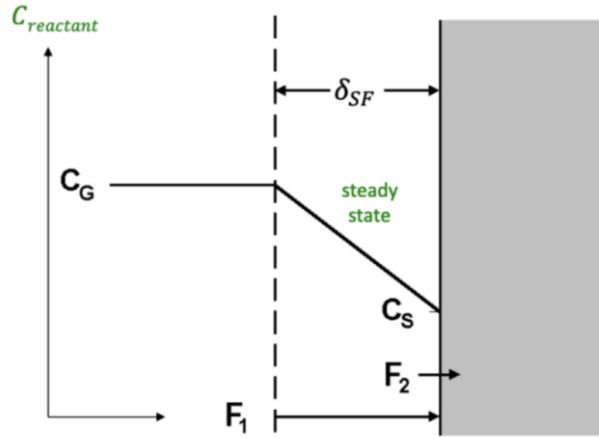


Figure 44: Process model diagram for chemical vapor deposition. There is a film of fluid that has zero velocity near the surface of the substrate, and so reactants must diffuse through this fluid. This is used for thin film deposition in the semiconductor industry, but is applicable to our experiment as well [37].

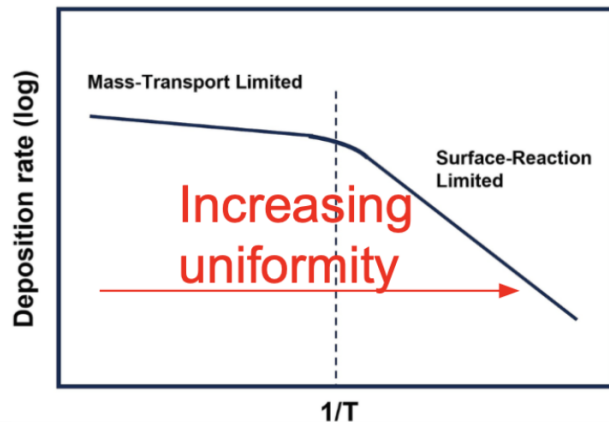


Figure 45: Deposition rate versus $1/T$, where T is temperature, for a Chemical Vapor Deposition process model. This is used for thin film deposition in the semiconductor industry, but is applicable to our experiment as well [37].

We completed two rounds of testing and obtained promising results for achieving a uniform PANI layer coating. Learnings from the testing were used to modify the test procedures after each round. We learned that conducting the reaction in a cooled environment to approach the reaction-rate limited regime was beneficial to achieving coalescence and a more uniform layer. Additionally, it may be beneficial to introduce a homogenized APS solution dropwise, rather than mixing all the chemicals at once.

It is important to note that the object to be coated was composed of a different material between round 1 and 2 of testing. In round 1, the object was made of smooth polystyrene (PS) plastic, whereas in round 2 it was 3D printed with Formlabs Biomed Resin, resulting in a slightly stickier and rougher surface texture. Additionally, several factors were changed simultaneously between each round of testing — including temperature, time, and material — so the ideal deposition time must still be determined with further testing.

Both rounds of testing used the following basic materials and equipment:

Table 9: Materials for PANI layer reaction

Material Name	Abbreviation	Quantity	SDS Warnings
Ammonium Persulfate	APS	5g	
Hydrochloric Acid	HCl	50mL	
Aniline	-	4mL	
Deionized Water	DI water	-	

Equipment:

- Pipet
- Weighing boat
- Scale
- Graduated cylinders
- Glass beakers
- Magnetic stirrer hot plate
- Magnetic stir bar
- Fume hood
- Object to coat
- Timer

Initial Test Procedure

Our initial testing procedure followed a heated environment and shorter deposition time, similarly to Shoukatch's paper. For the object to coat, we used small plastic vials made of smooth PS.

1. Clean a glass beaker with deionized water.
2. Use a weighing boat and scale to measure out 5 g of APS (see Figure 46).
3. Use a graduated cylinder to measure out 50 mL of HCl.
4. Use a pipet and small graduated cylinder to measure out 4mL of Aniline.
 - (a) Due to the toxicity of Aniline, first pour out a small quantity in a short beaker, jar, or other container with a wide enough opening for the pipet to fit.
 - (b) Use a pipet to carefully add 4 mL of Aniline to the graduated cylinder.
5. Add HCl, APS, and Aniline to the glass beaker cleaned in Step 1.
6. Place the beaker on the magnetic stirrer hot plate and place the magnetic stir bar in the beaker.
7. Turn on the magnetic stirrer hot plate. Set the temperature to 30°C and the stir rate to 100 RPM.
8. Let the solution stir for 1 minute at 100 RPM.
9. Place the object to be coated into the beaker with solution.
10. Increase the stir rate to 200 RPM and let stir for 10 minutes.

11. Take the object out of solution.
12. Into a different beaker, rinse the object with DI water.
13. Let the coated object dry overnight.



Figure 46: Chemicals used in the PANI layer deposition reaction. A weighing boat and scale was used to measure out 5g of APS.

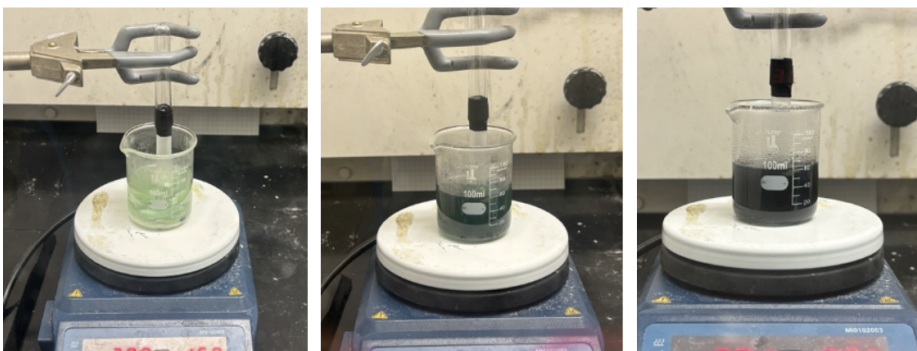


Figure 47: Experimental setup and evolution of PANI layer formation over 10 minutes of reaction. The solution color starts clear and gradually becomes dark green.

During the reaction, we observed that the reaction solution began as clear and eventually became dark green (see Figure 47) as the Aniline reacted with the HCl and APS and began to nucleate. This result aligned with that seen by the Prasad Lab [27]. After 10 minutes were complete, we removed the vial from the solution and noticed some nucleation. However, there was little growth and no coalescence into a uniform PANI layer, as shown in Figure 48. We realized that the methods outlined in Stoukatch's paper were oversimplified.

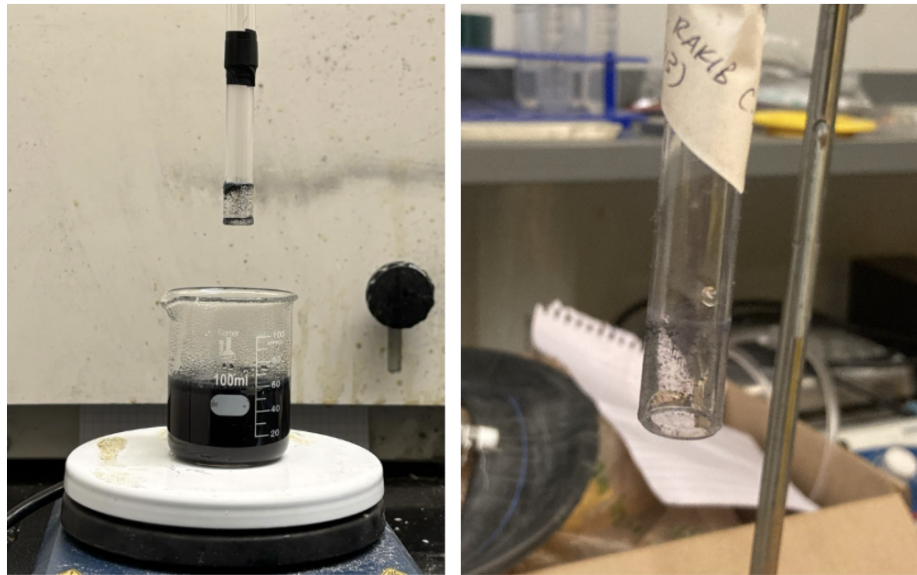


Figure 48: Results seen after pulling vial out of solution after 10 minutes of reaction time (left) and after rinsing the vial with DI water (right).

While few details or resulting images were shared in Stoukatch's paper for the PANI layer reaction, the video by the Prasad Lab showed clear results. We decided to adjust our test procedure to more closely align with that of the Prasad Lab to determine whether a cooler environment and longer deposition time might lead to better results.

We considered making the following changes for the next testing round:

1. Deposit the PANI layer in an actively cooled environment, instead of heated at 30°C, to push the reaction toward the reaction-rate limited regime. Consider using an ice bath, similarly to the Prasad Lab.
2. Increase the deposition time, checking at regular intervals to determine the time for which a uniform layer or minimum thickness is achieved. Consider that the Prasad Lab deposited for 1 hour.
3. Dissolve the APS into HCl before starting the reaction with aniline to improve uniformity.
4. Deposit on Nylon-12 for more accurate results since the material composition and surface finish of the object to be coated may have a significant effect on the result.

Refined Test Procedure

The second testing procedure followed a cooled environment and longer deposition times, similarly to the Prasad Lab. For the object to coat, we 3D printed 5 of our OD trenches from the base of our bioreactor vessel using Formlabs Biomed Resin Clear.

The following additional materials were required:

- 2 additional beakers, with one slightly larger than the reaction beaker
- Ice to actively cool the reaction beaker
- Tape

The refined test procedure was as follows:

1. Clean a glass beaker with deionized water. This will be the reaction beaker.
2. Prepare APS solution.

- (a) Use a weighing boat and scale to measure out 5 g of APS.
 - (b) Fill a different beaker with 50 mL of DI water.
 - (c) Add the APS to the beaker with DI water.
 - (d) Stir the solution until the APS has fully dissolved in the water.
3. Use a graduated cylinder to measure out 50 mL of HCl.
 4. Use a pipet and small graduated cylinder to measure out 4 mL of Aniline.
 - (a) Due to the toxicity of Aniline, first pour out a small quantity in a short beaker, jar, or other container with a wide enough opening for the pipet to fit.
 - (b) Use a pipet to carefully add 4 mL of Aniline to the graduated cylinder.
 5. Add HCl and Aniline to the reaction beaker.
 6. Fill a slightly larger glass beaker about halfway with water and add ice.
 7. Place the reaction beaker into the beaker with ice water.
 8. Use tape or other means to secure and stabilize the reaction beaker such that it does not get pushed up or tilted due to the ice water (see Figure 49).
 9. Place the beakers on the magnetic stirrer hot plate and place the magnetic stir bar into the reaction beaker.
 10. Add the 4 objects to be coated into the reaction beaker.
 11. Turn on the magnetic stirrer hot plate. Set the stir rate to 170 RPM.
 12. While the solution stirs, gradually add in the APS solution from Step 2 (see Figure 49).
 13. Take out one object after 30 min, 40 min, 50 min, and 60 min.
 14. For each object, into a waste beaker, rinse the object with DI water.
 15. Once all objects have been removed, add the last object to be coated into the beaker.
 16. Let stir for 20 min, taking the object out of solution to check PANI nucleation at regular intervals.
 17. Take the object out and rinse with DI water into the waste beaker (see Figure 50).
 18. Let the coated objects dry overnight.

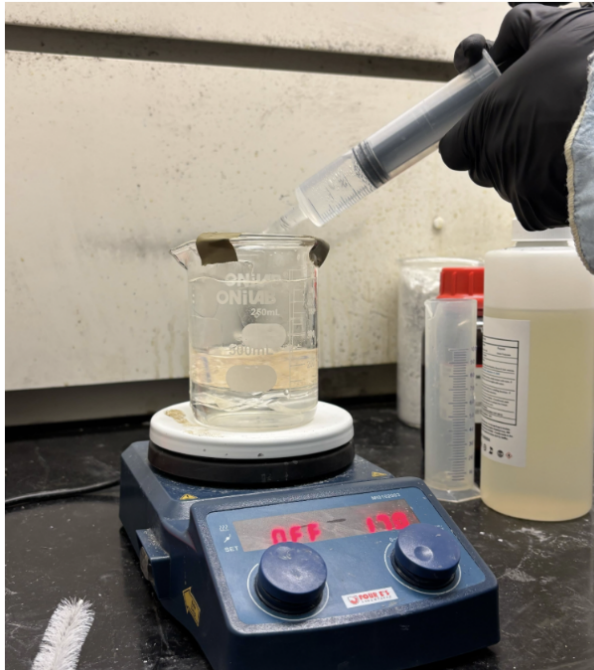


Figure 49: The reaction beaker sits inside a slightly larger beaker filled with ice water. Tape is used to secure the reaction beaker to the outer beaker and prevent it from bobbing or tilting due to the ice water. APS solution is gradually added into the reaction beaker.

For Step 12, we initially used a syringe to add the APS solution dropwise, similarly to the method of the Prasad Lab. However, partway through the process, we changed to gradually pouring the APS solution directly from its beaker. Due to the less gradual introduction of APS solution into the reaction, this may have harmed the uniformity of the resulting film, although this has not been confirmed.

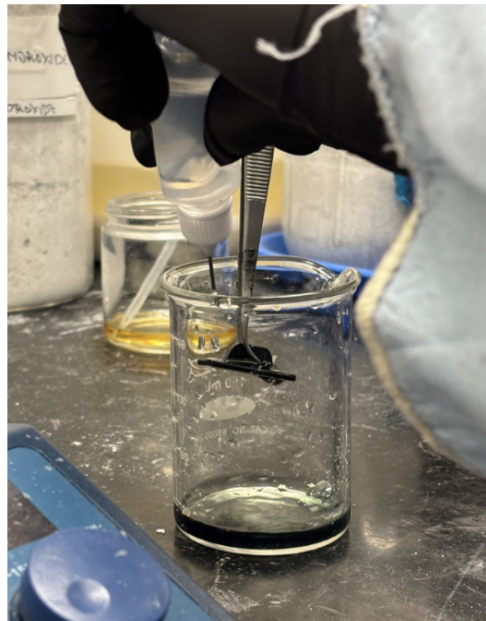


Figure 50: A squirt bottle was used to carefully rinse one of the first four coated parts with DI water.

Once the first four samples were done reacting, we added in a fifth sample according to Step 15 of the refined test procedure. Since the previous four samples had already formed a uniform coating within 30 minutes, we believed the time required to form the coating was less than 30 minutes and wanted to test this with the fifth sample. We took the sample out to check PANI nucleation after 5, 10, 15, and 20 minutes (see Figure 51).

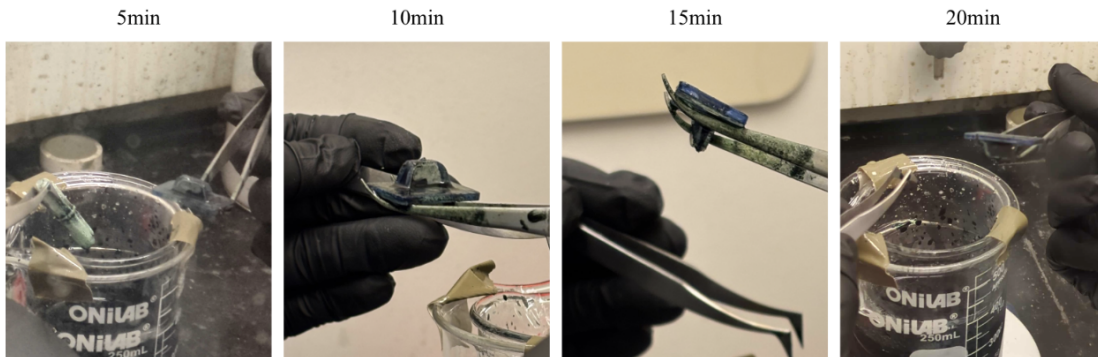


Figure 51: The fifth sample after 5, 10, 15, and 20 minutes of reaction time.

The lack of significant coalescence after 20 minutes led us to believe that the polymerization reaction of the aniline monomers had almost completely finished during the process of coating the first 4 samples. Additionally, like in our initial test round, the fifth sample was placed after the reaction had already begun. Therefore, we believe placing the object in solution before beginning the reaction is a crucial factor in achieving a uniform coating. Further, it may be helpful to increase the duration of time spent adding the APS solution dropwise to slow the reaction and lead to a more uniform film.



Figure 52: All five samples after PANI layer deposition. The less nucleated sample (left) is the fifth sample, which was reacted after the four below it (Step 15-17). The four darker samples show uniform PANI layer coating and were reacted for 30, 40, 50, and 60 minutes from left to right, respectively.

Upon visual inspection, the samples at 30, 40, 50, and 60 minutes all appear the same, as shown in Figure 52. Thus, for a more accurate analysis of the results each sample should be cut to expose the cross section of the coated object and a microscope should be used to measure the thickness of the coating. If the thicknesses are the same (or very similar), this would lead us to conclude that the polymerization reaction of the aniline monomers had almost completely finished by 30 minutes. Therefore, the reaction duration can likely be shortened, though the extent of this is unknown and would require further testing. Additionally, if the thickness under microscope appears to be non-uniform, it may be beneficial to increase the duration of time spent adding the APS solution dropwise, to slow the reaction and lead to a more uniform film.

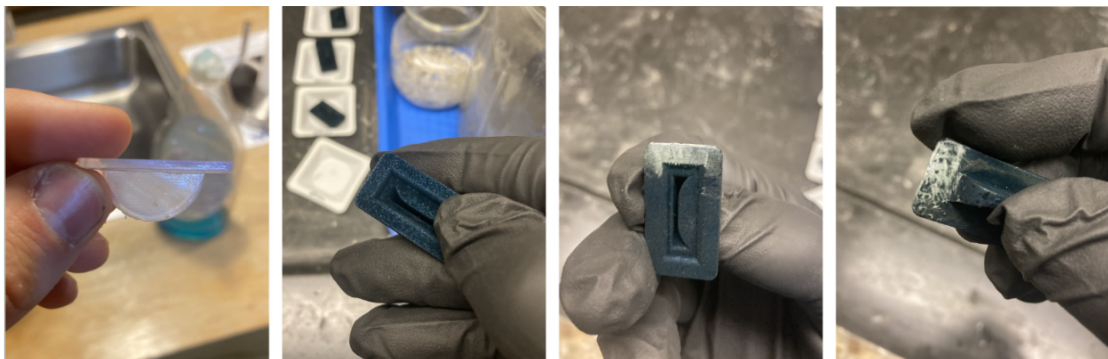


Figure 53: Formlabs part before reaction (left) compared to the sample after 30 minutes of reaction. The PANI layer can be scratched off using a pair of metal tweezers to expose the original surface.

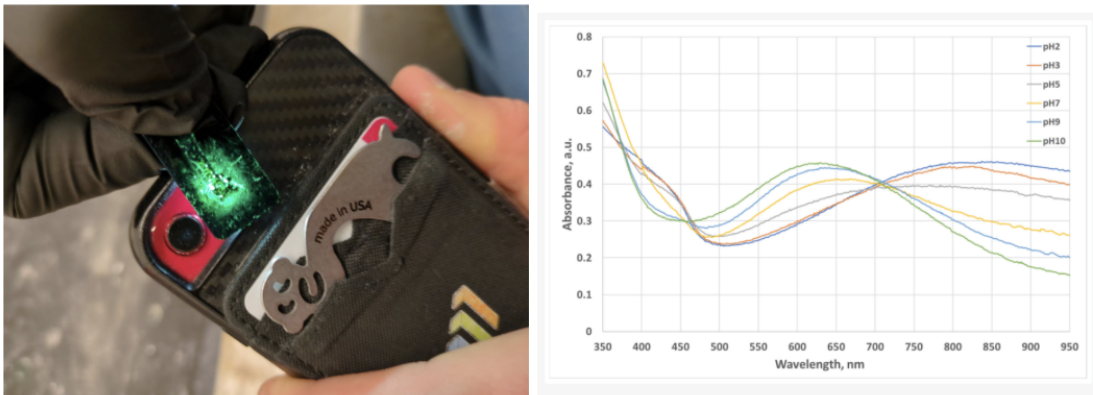


Figure 54: Quick test for light read-through using a white LED iPhone flash. Despite being a dark opaque color, the layer is somewhat transparent to light, which appears green as it passes through the layer. This makes sense because the PANI layer has its lowest theoretical absorbance to green light, as shown in the reproduced figure to the right (from Section 4.2).

The next step is to cut our samples in half and look at the cross section with an optical microscope. We need to determine the film thickness and look for any differences in microstructure to determine the ideal reaction time and uniformity. If we are correct with our interpretations from the figures, we consider making the following changes for the next testing round:

1. Add the entire APS solution dropwise.
2. Experiment with shorter deposition times, between 10-40 minutes.
3. Experiment with Nylon-12 instead of Formlabs Biomed Resin to match the intended vessel material.
4. Experiment with masking techniques to contain the PANI layer deposition to the desired area on the inside of the trenches.
 - (a) Can tape be used to effectively “mask” off an area from the reaction?
5. Test the optical response to changes in pH with an LED and photodiode.
6. Use a pH probe to benchmark the results seen with our sensing technique to a device that is known to work.

4.6.2 DO Ruthenium Layer

In this semester, we did not get a chance to synthesize the ruthenium complex layer. Our plan for this was to loosely follow the steps laid out in the previous demonstration of this sensor, whereby we create a Sol-gel based dye [5]:

1. Magnetically stir ethanol with Ru(dpp)³Cl₂, this forms the indicator solution.
2. Sol-gel prepared through hydrolysis with TEOS and water (We recommend watching this video [22] for a good overview of the process)
3. 10g of this silica gel is stirred with 10mL of the ethanol solution of Ru (II) and heated until the gel absorbs the indicator. We are not sure of the parameters (time, temperature). You will need to do some searching of literature or consult a chemist.
4. Silicone resin is used to place these beads onto the sensor spot in the reactor chamber.
5. The gel is allowed to dry for 2 days.

6. Test with LED and photodiode, replicating the expected output in 4.3.

Table 10: Materials for Ruthenium Complex reaction

Material Name	Abbreviation	SDS Warnings
Tetraethyl Orthosilicate	TEOS	 
Silicone Adhesive	HCl	 
Tris(4,7-diphenyl-1,10-phenanthroline)ruthenium(II) dichloride	Ru(dpp) ³ Cl ₂	
Ethanol	Ethanol	 
Deionized Water	DI water	

5 Electronics

NIMBLE's electronics consists of three parts: power electronics, transducer manipulation, and signal processing that are all controlled using a Raspberry Pi 5. The power electronics are used to provide power to various components in the bioreactor that can't be supplied by the Raspberry Pi. The transducer manipulation primarily consists of gate drivers used to control the motors and heater system. The signal processing is critical to properly sending and receiving data to and from the sensors to allow for feedback control, reliable measurement, and noiseless data. The electronics system is designed to be implemented in a laboratory setting with a 120V standard wall outlet.

5.1 Power Electronics

The power electronics circuitry is used to receive power from a wall outlet and distribute it as needed to the Raspberry Pi which requires 5V, the motors which require 12V, and the heater system which also requires 12V. This is done through a series of linear power supplies starting with a standard AC to DC converter. In order to determine what components are needed in our system, an estimated power consumption was calculated given thermal demands, typical current draws found online, and known resistances. As seen in Table 11, NIMBLE operates at an estimated continuous power draw of 16W while having the potential to reach up to 60W which is the expectation we should specify our components to.

Table 11: System power consumption.

Component	Peak Power (W)	Equilibrium Power (W)
Resistive Heater	20	11
Stirring	1	1
Pumps	5	0.5
Sensors	0.2	1
Raspberry Pi	25	2.7
Touchscreen	0.65	0.65
Total	60W	16W

NIMBLE uses a 12V, 5A Power Supply seen on Figure 55 to provide a base 12V to the system. This converter was selected given the 12V had to sustain minimal voltage ripple (4-5%), meet the needed max power requirements, and allow for protection features such as thermal overload protection, over-voltage protection, and galvanic isolation. The converter offers a maximum power output of 60W which is well above our estimated power draw. It also features a 90% typical efficiency in addition to power overload, overvoltage, and over temperature protection [21].



Figure 55: 12V 5A AC/DC Converter manufactured by Mean Well

From the 12V, the electrical system distributes 5V to needed logic components and the Raspberry Pi. Since the 12V to 5V linear power supply has significantly lower power consumption (25W peak for the Raspberry Pi), a single chip with a heatsink can be used. This design implements the LM1084 as it can

provide 5A at 5V with a 0.1% typical load regulation [20]. This chip is typically used in a 5V regulated circuit that is provided in its datasheet as shown in Figure 56. This provided circuit contains an input capacitor to filter input noise and stabilize input voltage, an output capacitor to improve transient response and stability, a voltage divider for output voltage adjustment, and a bypass capacitor to prevent voltage ripple.

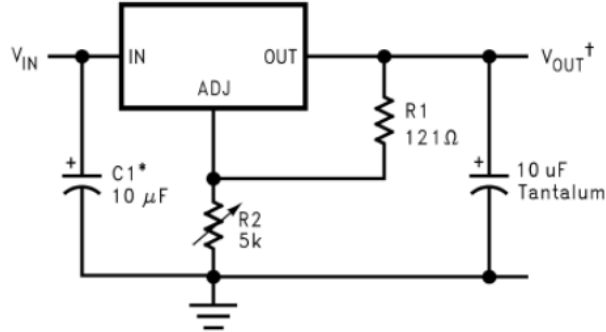


Figure 56: LM1084 recommended 5V application circuit.

5.2 Gate Drivers

The actuator system of the bioreactor provides power to 3 input motors, one output motor, a brushless stirring motor, and a heating element. This system has several key design requirements:

- Provide stable 12V input
- Supply sufficient current for each motor/heating element
- Handle total power output specified in Figure X
- Maintain efficiency to minimize heat generation
- Offer protection against short circuits

The system includes three peristaltic pumps in addition to a silicone heating device which encapsulates the fluid management and temperature control. All four of these components are designed to be powered using direct current (DC), and their power delivery is managed using a DC driver circuit. While there exist a number of ways to implement a DC actuator driver, such as placing a MOSFET directly between the power source and the load, such methods often limit circuit efficiency and frequency capabilities. To counteract these issues, the design implements a “totem pole” circuit as shown in Figure 57. This configuration of gate drivers is particularly well-suited to provide fine actuator control for applications in biomedical research or chemical processing.

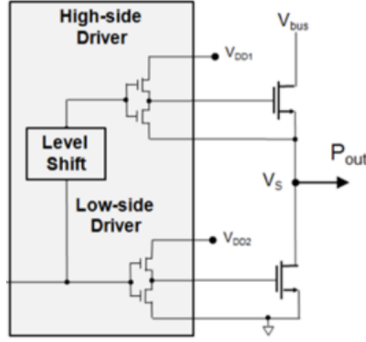


Figure 57: Totem Pole Diagram

The totem pole circuit configuration offers many advantages over a single-MOSFET configuration. This circuit architecture utilizes two MOSFETs: a high side driver which ties the load to the voltage source in addition to a low side driver which ties the load to ground. These MOSFETs are powered independently from the actuator elements. This separation allows for higher efficiency while also maintaining switching performance. The independent power supply allows for faster switching by always providing adequate gate driver signals even while source voltages fluctuate. This reduces switching losses, which is particularly important when implementing high speed control systems to operate pumps and heaters that require precise response. In contrast, a single MOSFET would likely require overdesign due to requiring higher ratings than strictly necessary to ensure reliable operation under varying load conditions.

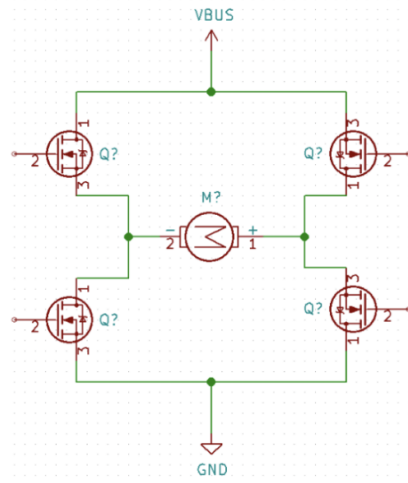


Figure 58: H-Bridge Working Principle Diagram

Putting two totem poles together gives us the circuit shown in Figure 58, which is commonly known as an H-Bridge. This circuit is implemented using an off the shelf L298N integrated circuit. The H-Bridge configuration gives us the benefits previously listed of the totem pole circuit but enables the circuit to be easily scalable and enable the function of direction change.

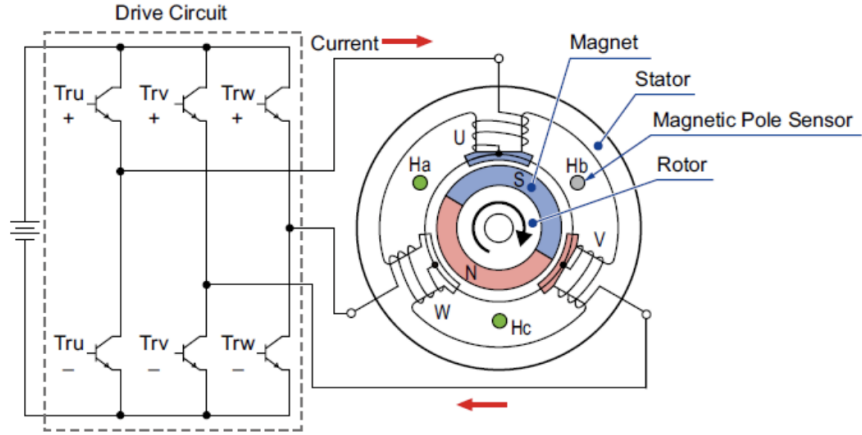


Figure 59: Simplified Brushless Motor Model

Motor control for the brushless stirring motor, however, requires a particular switching sequence to drive motor windings. The configuration of a brushless motor is shown above in Figure 59. The key components are:

1. **Stator:** The stationary part of the motor which consists of windings arranged in a particular pattern. Current flowing through these windings generates a rotating magnetic field.
2. **Rotor:** The rotating part of the motor which holds permanent magnets. The magnetic poles of the permanent magnets interact with the windings of the stator.
3. **Electronic Controller:** Manages electronic commutation as opposed to the brushes which act as the commutator for a DC motor.

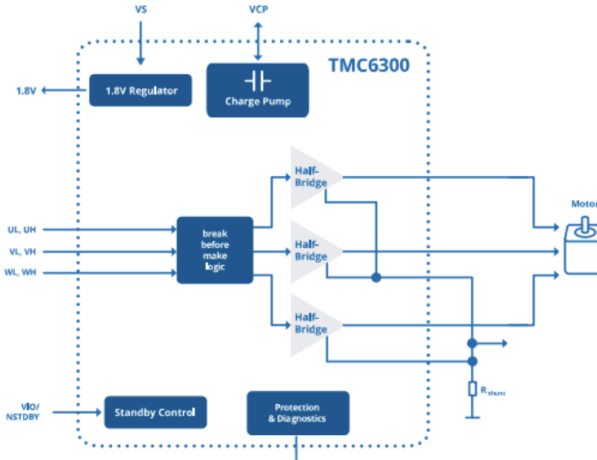


Figure 60: TMC6300

Figure 60 shows an example of the electronic controllers mentioned above as key components of the function of brushless motors. These controllers utilize advanced logic designs to precisely manage current flow through the motor windings to achieve the same function as a physical commutator in a typical DC motor. Two key components of this logic circuit are the “break before make” logic in addition to the “half bridge”, which serve the same function as the “totem pole” circuits described earlier. The “break before make” logic is important in ensuring that the high-side and low-side switches do not activate simultaneously, which would cause shoot-through from power to ground, damaging the electronic components.

Putting three of these circuits together allow for the direction and timing of the windings to be controlled using the logic sequence as shown above. When the electronic controller above sends current through specific rotor windings in the determined logic sequence, a magnetic field is created. The rotor aligns itself with this magnetic field, which is also rotating. The electronic controller constantly adjusts this logic sequence such that the rotor is always “chasing” the magnetic field of the stator and ensuring that the magnetic field is constantly pulling on the rotor in the desired direction.

Speed and direction of the brushless motor is determined by changing the voltage that is supplied to the motor windings through PWM. Adjusting the duty cycle of this PWM signal allows the motor controller to vary the average voltage being applied to the motor windings, allowing speed control using a control algorithm. Additionally, modifying the sequence by which the windings are activated can allow easy reversal of motor direction, which will allow stirring in both directions to accommodate various stirring designs.

Because the stirring motor is running nearly at all times, the advantages of brushless operation are clear in their implementation. The absence of brushes and the replacement with electronic commutation reduce any friction related energy losses significantly and improves overall efficiency. The electronic commutator also leads to a much longer operational lifespan because of the lack of mechanical brushes which would need to be serviced or replaced. The brushless stirring motor will also make less noise and vibration. In this particular application with continuous use over 2 weeks, reduction in noise and vibration is beneficial for operational comfort.

5.3 Analog Signal Input, Data, and Filtering

As part of having functional sensors, care must be taken to ensure that the correct voltages, signals, and power is going in and out of the various sensor components. This includes noise reduction, analog conversion, and use of a multiplexer to access the large number of components. To do these tasks, a custom Printed Circuit Board (PCB) called the “Breakout Board” is implemented which routes, filters, and powers the needed components. Due to time constraints, this board was only designed schematically as shown in figure 61.

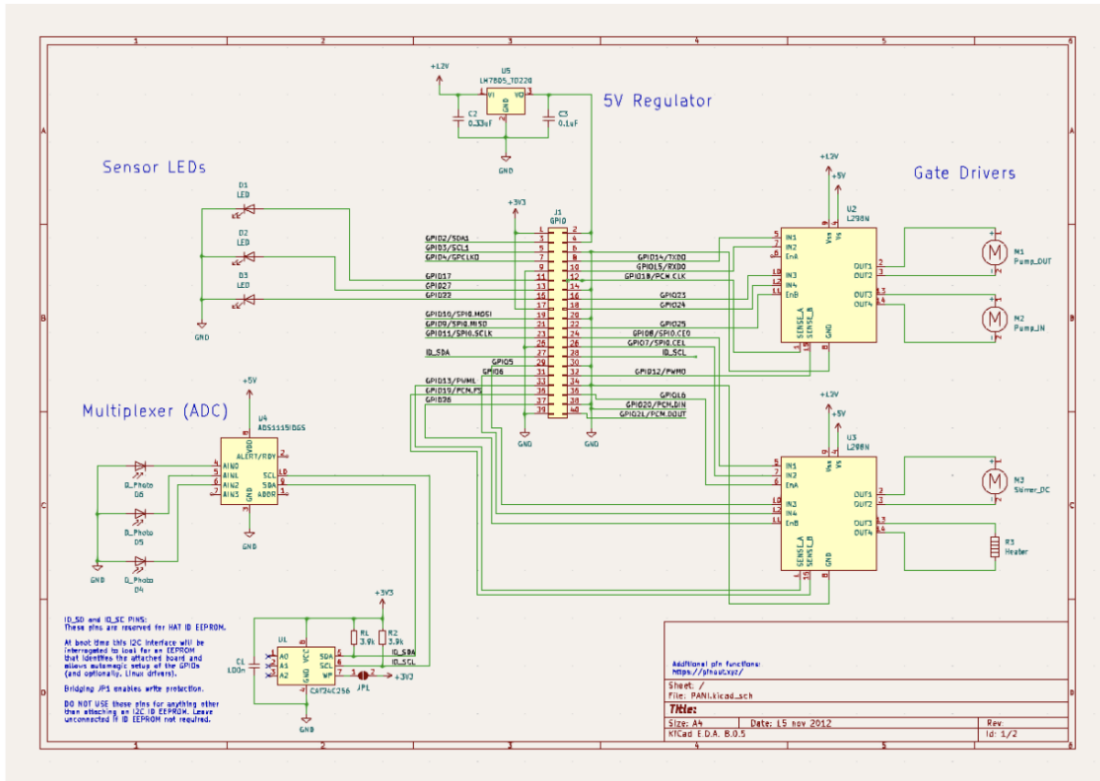


Figure 61: Proposed “Breakout Board” used to route, filter, and manage transducers.

As mentioned previously in discussion of sensors, some sensors need converting from current to voltage. In addition to this conversion, these signals also need to be converted to values that the Raspberry Pi can process. This is done using an ADS1115 ADC and a MCP3008 multiplexer as shown in Figure 62.

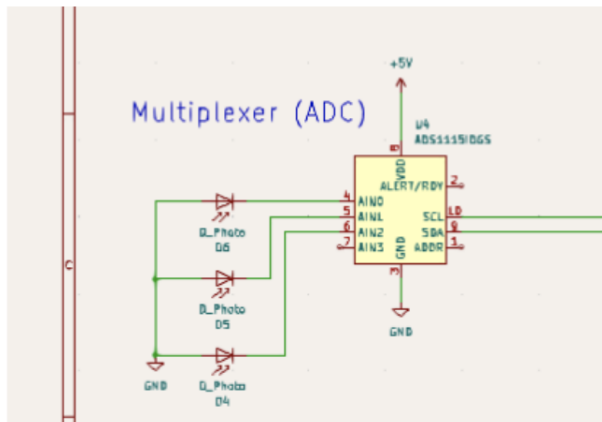


Figure 62: Schematic of multiplexer and ADC implementation

In addition to what's shown in the Breakout Board, data needs to be routed into an SD card as well to provide users with logging of the data that is collected. This is done through the Raspberry Pi and onto an SD card which is located in the memory space of the Raspberry Pi. A block diagram of data flow is shown in Figure 63.

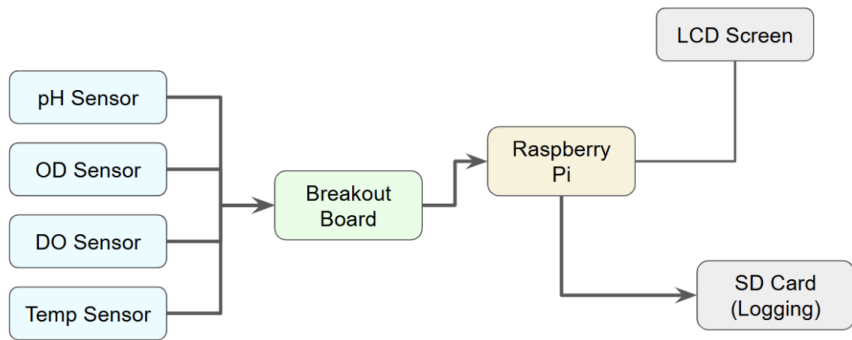


Figure 63: Block diagram of data flow throughout the electrical system.

6 Environment Control

A control system is required to maintain the temperature, pH and dissolved oxygen requirements inside the bioreactor. Depending on what reactions are occurring inside the vessel, the consumed reactants and resulting products will influence the pH levels, produce heat and affect gas levels [6]. The goal of the bioreactor is to be completely autonomous to minimize user involvement as the reaction occurs.

A survey of industry control schemes revealed control methods ranging in complexity. The most complex uses Model Predictive Control (MPC). MPC models the growth of the culture, the rate of reactions and predicts the system response so that the controller may respond more accurately [16]. Other methods utilize closed loop PID control using a simplified model to develop the system transfer function.

6.1 Temperature Control

The model developed in Section 2 is used and shown in Figure 64. A thermal resistor network models conduction from the heater through the wall and convection between the wall and the water circulating inside the vessel. If there is any exposed surface between the vessel and ambient air, there will also be an additional convection term. This term is neglected for now. The relationship between temperature, heat transfer and thermal resistance is shown in Equation 26.

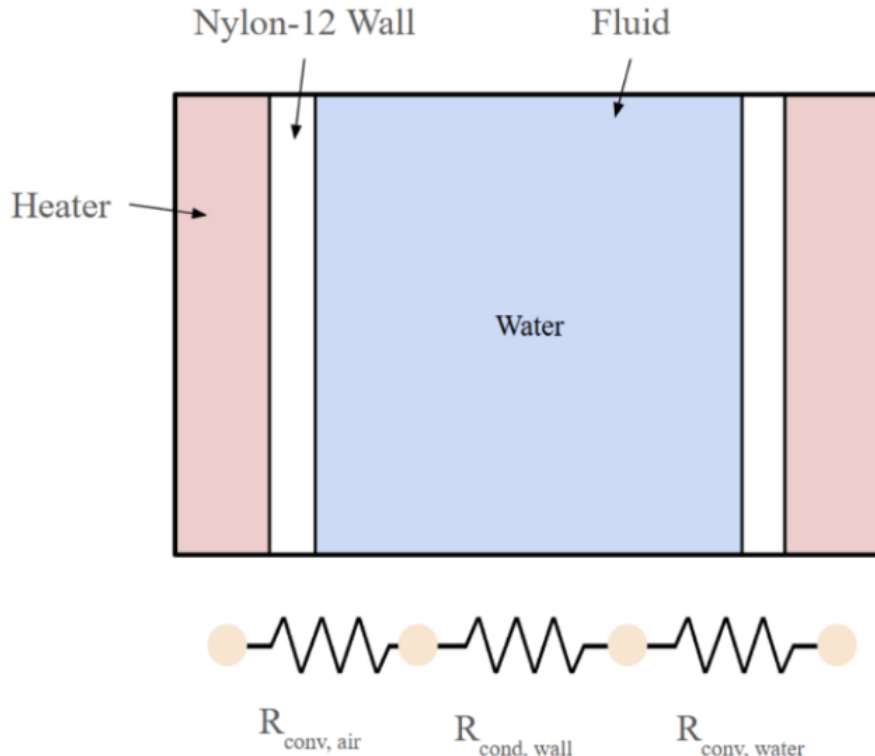


Figure 64: Simple thermal resistance network for bioreactor. $R_{\text{conv},\text{air}}$ is neglected assuming no air gap between heater and vessel.

$$\Delta T = \dot{Q} \times R_{\text{eff}} \quad (26)$$

Newton's first law of thermodynamics governs the conservation of energy, shown in Equation 27. It states the change in energy is equivalent to the sum of heat transfer into and out of the system and work done on and by the system.

$$\frac{dE}{dt} = \dot{Q} - \dot{W} \quad (27)$$

The change in energy of the bioreactor is equivalent to the change in thermal energy by the water:

$$\frac{dE}{dt} = m_w c_{p,w} \frac{dT}{dt} \quad (28)$$

Plugging Equation 26 and Equation 28 into Equation 27 yields the following governing differential equation:

$$m_w c_{p,w} \frac{dT}{dt} - \frac{1}{R_{eff}} \times T(t) = -\dot{W} \quad (29)$$

Where $T(t)$ is defined as the difference between ambient and the water for simplifying algebra. Converting from the time domain to the S-domain and rearranging yields the first-order system open loop transfer function:

$$H(s) = \frac{T(s)}{W(s)} = \frac{1}{m_w c_{p,w} s - \frac{1}{R_{eff}}} \quad (30)$$

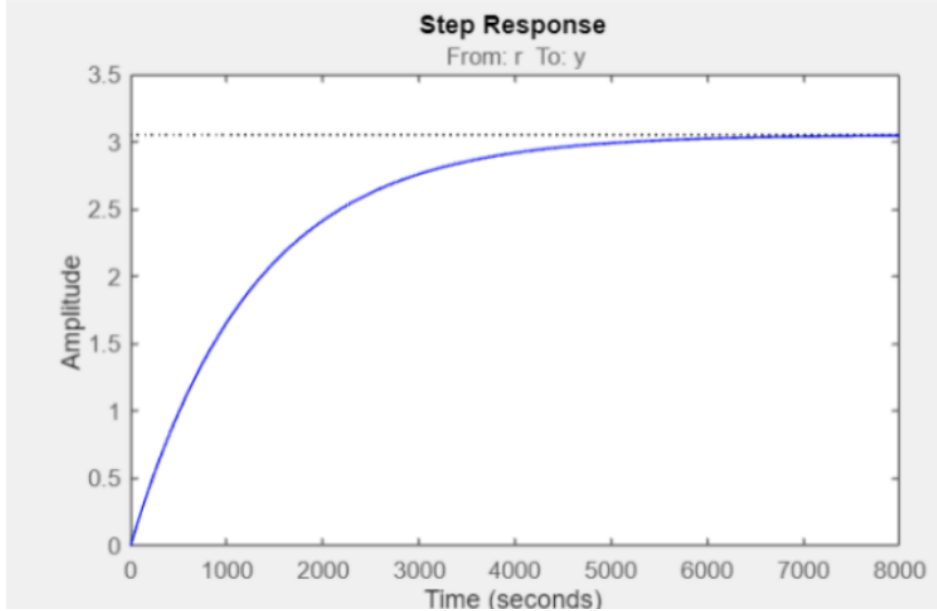


Figure 65: Step response of open loop temperature response in bioreactor after power input. Curve is characteristic of first-order systems following the function.

The time response from a step input is shown in Figure 65. The y-axis represents the temperature difference between ambient and vessel temperature. The x-axis is time. The time constant for the system to reach 63% of the final value is about 1200s or 20 min. To clarify, this is not the final time required to heat the bioreactor, but instead is a characteristic time for the system to reach equilibrium after a temperature disturbance.

The important takeaway from Figure 65 is there is no overshoot and there are no oscillations around the equilibrium point. These observations are characteristic of first-order systems and benefit the control problem. However, there is a 13% steady state error. A proportional-integral closed loop feedback controller is required to control the system to the given temperature requirement of ± 0.5 C. The step response of the closed loop PI transfer function is shown in Figure 66:

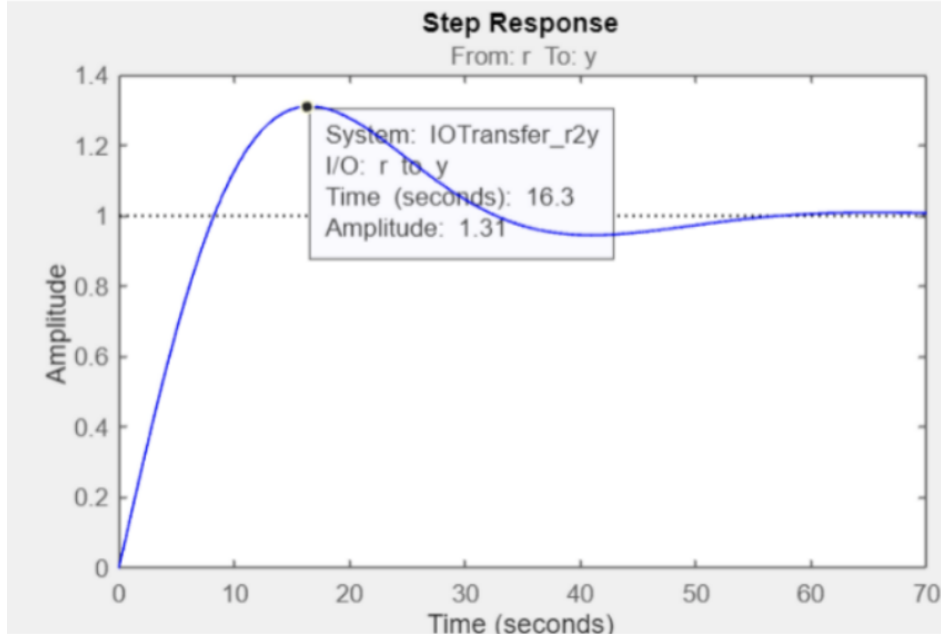


Figure 66: Closed loop response of the PI transfer function. The time constant τ is 8s and the overshoot is 31%. We do not have an overshoot specification because there will be a 10 minute time for the vessel to heat up and stabilize before starting the reaction.

To increase precision of control, the temperatures of inlets, outlets and culture production can also be modeled. This leads to more complex control requiring full PID [15]. Since our vessel is much smaller, a proportional controller will be pursued for now. If it proves insufficient during testing, a more complex scheme will be developed.

6.2 pH Control

The pH is controlled by addition of acids and/or bases. The user can decide between two-sided control, with acid and base addition, or one-sided control, with only one of acid or base addition to regulate processes that drift toward high or low pH over time. The user will input a target pH and a tolerance level, as well as a cycle time in seconds. The cycle time determines the frequency of pH adjustment, and is independent of the frequency of pH measurement, which will occur every 30 sec.

The pH control approach consists of a closed-loop feedback on-off controller (also known as a bang-bang controller) with a deadband. Each time the cycle time has elapsed, the measured pH value is compared with the target pH range, as determined by the user inputs. If the current pH is outside the tolerated range, the acid or base pump will be activated to add a fixed volume of acid or base to bring the pH within range. This control scheme is illustrated in Figure 67. The peristaltic pumps are not designed to pump a specific volume of fluid, but rather to pump at a certain flow rate, so using them to pump a certain fixed volume of acid/base could be difficult. However, knowing the exact volume will not be necessary for the reasons listed below. The implementation of this pH control system is largely adapted from a similar method found in a recent study [18].

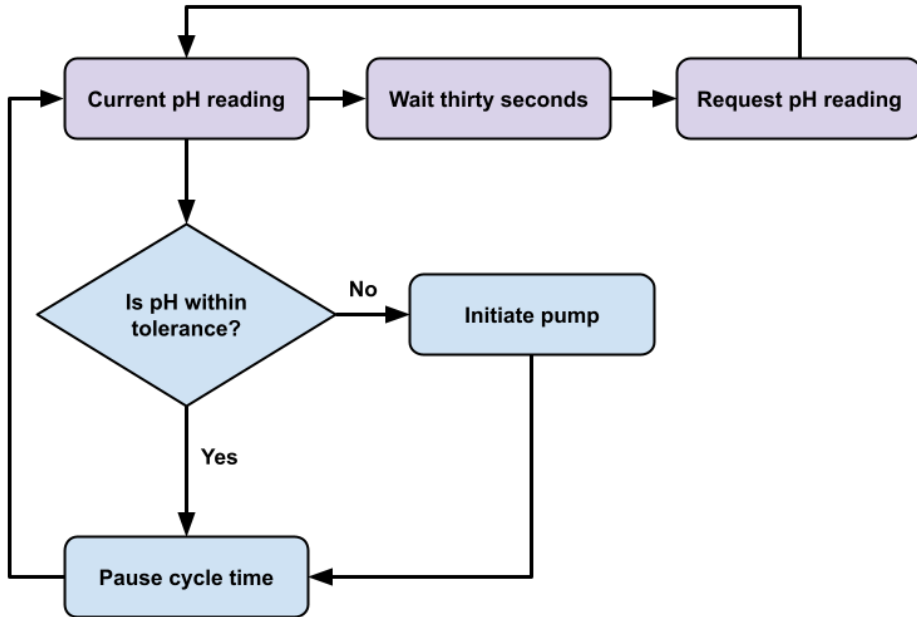


Figure 67: Decision tree illustrating the pH measurement function integrated into the digital bus and hardware (upper horizontal flow cycle), and the function for the control of pH according to a predefined tolerance of a pH set point (lower cycle) [18].

The volume of added acid or base needed to bring the pH of a solution to a certain value is dependent on a lot of different factors. These factors include the buffering capacity of the solution, the strength of the acid/base, metabolic byproducts of the reaction, and other non-ideal behaviors. Due to the fact that many of these factors depend on the specific reaction that is taking place and other decisions that will be made by the user of the bioreactor, we cannot determine algorithmically how much acid/base should be added to control the pH. Therefore, when the pH needs to be adjusted, we will pump a small amount of acid/base by sending a quick on/off command to the pump. The bioreactor has a relatively small volume of 100mL, so a quick pump of acid/base should be enough to adjust the pH by a small amount. If the pH still is not within the target range, it will be adjusted further in the next control cycle.

6.3 Dissolved Oxygen Control

The control scheme used to monitor and adjust the dissolved oxygen content of the system is similar to that of the pH control in Section 6.2. It utilizes a closed-loop feedback on-off controller to add oxygen when the measured DO is below the target range. The system will have several possible gas inputs, depending on the needs of the reaction, however only dissolved oxygen will have active control. The user will input the desired quantity of dissolved oxygen and the system will automatically maintain that value with the feedback controller. Similarly to the pH control scheme, each time a control cycle occurs, a small fixed amount of oxygen will be added to the system. At the next control cycle, if the dissolved oxygen content has still not reached the desired range, more oxygen will be added, and this will repeat until the desired range is reached.

6.4 Environment Control Future Work

The controls system has been modeled and designed but yet to be implemented or tested. Testing the control systems is crucial to validating the models and tuning them based on real world conditions. Proposed future work includes:

- Test PI temp controller with heater and thermistor

- Correlate to time-response model
 - May need to remodel system if unaccounted for factors cause error (such as reaction heat production)
- Measure passive cooling rate and add to thermal model if necessary
- Test bang-bang pH controller
- Test bang-bang DO controller
 - Less crucial to overall design of product since gas box is an add-on

7 Vessel and Structure Design

Structures house the electronics and the disposable reaction vessel, along with the interfaces between the two. The current design of the electronics packaging is our preliminary packaging approach and will evolve as our prototyping dials in the geometry of our sensors. The goal for this subsystem is to create a structure onto which all of the sensors and electronics can be mounted and operate during regular operation, along with providing a sealed, biocompatible environment for reactions to take place.

7.1 Reaction Vessel Overview

The reaction vessel is a crucial component of the bioreactor system, designed to maintain a 100mL reaction volume with optimal reactant homogeneity. Its basic geometry features a baffled cylinder design to minimize stagnant flow areas, with exterior keying for poka-yoke implementation and heating element mounting. A key innovation in this design is the inclusion of three "trenches" or pockets that enable noninvasive sensing, providing thin, representative samples of reactor conditions optimized based on thermofluids team simulations. The lid serves as the central hub for inputs and outputs, featuring one fluid input, four gas inputs, and one bottom-draw output for efficient material removal, along with a keyed connection for an Es-Motor 24mm brushless DC motor. Material selection was critical, with Nylon-12 chosen for its 90% visible light transmission in the 380-700 nm range, biocompatibility, and suitability for both 3D printing and injection molding. For prototyping purposes, Formlabs Biomed Clear Resin is being used. This comprehensive design ensures efficient mixing, easy monitoring, and biocompatibility, making the reaction vessel suitable for a wide range of bioreactor applications.

7.1.1 Basic Geometry

As specified by our sponsor, the vessel must have a 100mL reaction volume and maintain reactant homogeneity throughout the reaction process. The geometry of the vessel was driven by the need to maintain homogeneity throughout the fluid and being manufacturable through standard mass manufacturing methods. The geometry was chosen to be a baffled cylinder to minimize areas of stagnant flow in the vessel. For further information about fluid flow within the vessel refer to Section 3.5.

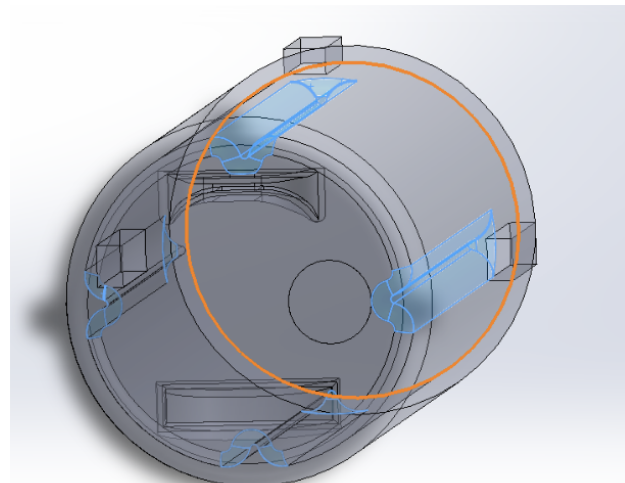


Figure 68: Turbulence-inducing baffles highlighted in blue.

The outside of the reaction vessel is keyed to practice poka-yoke in both its mating to the base structure and the mounting of the heating element. This design approach uses physical features to prevent incorrect assembly, ensuring that components can only be connected in the correct way. By incorporating these mistake-proofing elements, the reaction vessel's design minimizes the risk of errors during setup and operation, enhancing overall efficiency and reliability in the bioreactor system.

7.1.2 Trenches

The key to our product is the ability to sense noninvasively. To make this possible we added three pockets we refer to as “trenches,” to create samples of reactant that we can sense through and monitor the conditions of the bioreactor as a whole. The design of the trenches was driven by the various requirements of the sensing team to have a thin, representative sample of the greater conditions in the reaction vessel. The thermofluids analysis informed the design of the trenches through fluid simulations (Section 3.5). As for specifics about the functions of the individual trenches, refer to Section 4 of the paper.

7.1.3 Lid

The lid of the reaction vessel serves as the nexus for all the inputs and outputs of the reactor. There is one fluid input, four gas inputs, and one output. All of the inputs & outputs are barbed to allow for quick connection to auxiliary equipment. The output draws fluid from the bottom of the vessel to allow for material removal no matter the internal level. The lid features a keyed connection for a Es-Motor 24mm brushless DC motor to connect to the stir bar via a set screw.

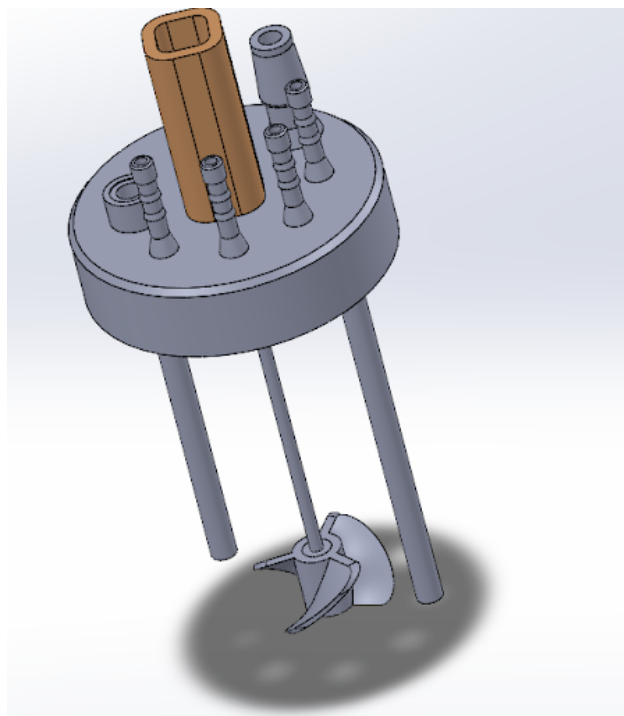


Figure 69: Lid with motor connection highlighted in orange.



Figure 70: Es-Motor 24mm brushless DC motor used for agitation spinner.

7.1.4 Material Selection

The material we selected to manufacture the vessel from had to be transparent in the visible light spectrum, biocompatible, and a viable option to manufacture in addition to being easy to prototype with. We selected Nylon-12 as it transmits 90% of visible light in the 380 -700nm range [?]. Nylon-12 is biocompatible, and can be 3D printed or injection molded. Nylon-12 was the most expensive material we evaluated, especially when compared to materials like PLA, but its superior biocompatibility made it the clear choice. Per vessel, the cost of using Nylon-12 as opposed to PLA is less than \$0.50.

Table 12: Material options and their viability.

Material	Transparency	Biocompatible	Environmental Resistance	Injection Moldable	3D Printable
ABS	✓	✗	✓	✓	✓
PLA	✓	✓	✗	✓	✓
Nylon-12	✓	✓	✓	✓	✓
TPU	✗	✓	✓	✓	✓

For our prototyping we have been using Formlabs's Biomed Clear Resin as it also fulfilled our design specifications and we have access to rapid prototyping through formlabs at the moment, allowing us to carry out our validation procedures. Figures 71 through 74 show our prototypes. The first figure shows the full bioreactor system assembly. The second figure shows the reaction vessel fitted into the sensing base. The third image shows the geometry of the sensing base in greater detail. And the final figure shows the geometry of the trenches on the vessel.

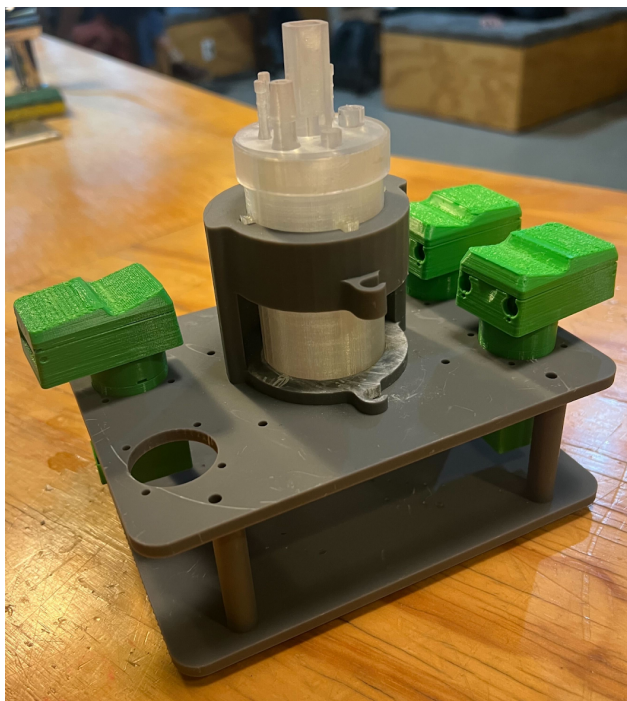


Figure 71: Full bioreactor 3D printed prototype.



Figure 72: Bioreactor base prototype with vessel prototype attached in trench grooves.

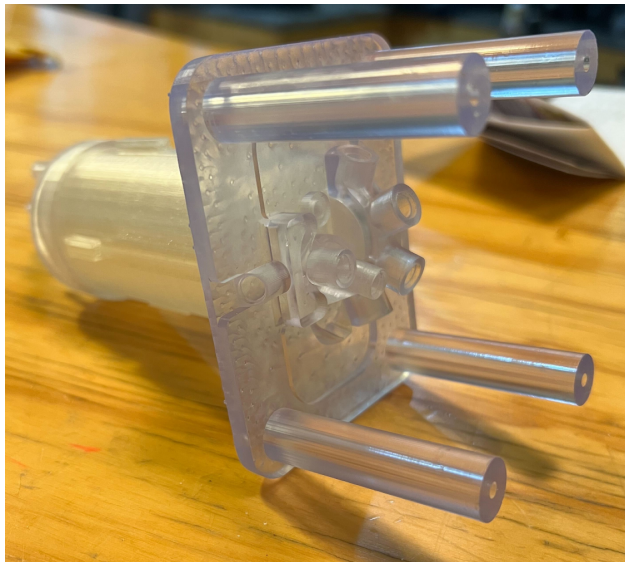


Figure 73: Bottom of bioreactor base prototype showcasing sensor architecture.



Figure 74: Vessel prototype bottom view.

7.2 Reusable Base

7.2.1 Overview

The base shown in Figure 72 is responsible for locating the vessel within the system, as well as being the primary mounting point for most components of the system including the vessel, heater, pumps, and sensor package. The vessel sleeve fits around the vessel, and provides a poka-yoke system to prevent incorrect placement of the vessel within the system. This is optional as the sensor packaging is also keyed, and is responsible for providing a hard stop for the vessel when inserted. The keys in the sleeve make the correct alignment clearer to a user, but are not strictly necessary.

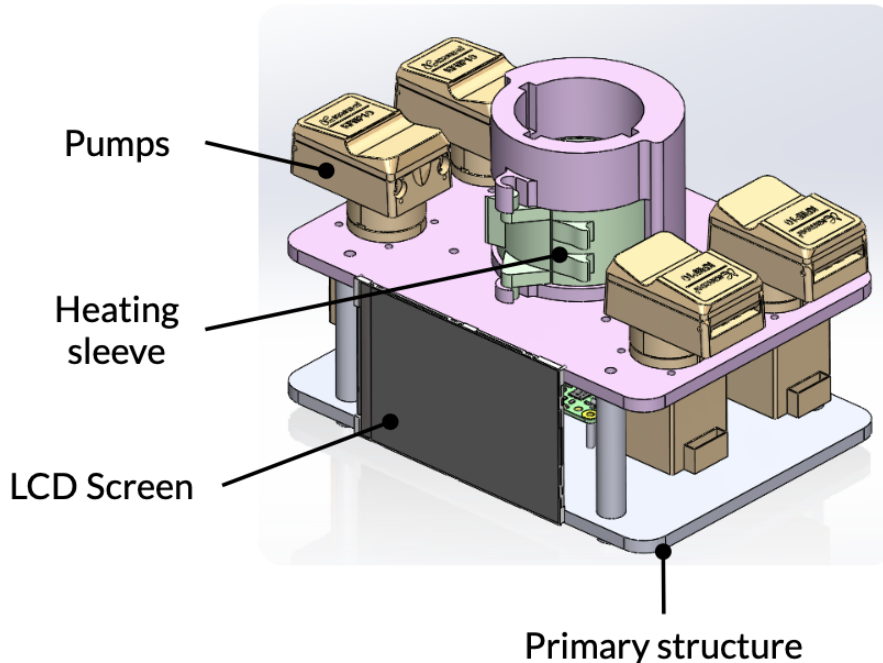


Figure 75: Full assembly of reusable components.

The pumps are mounted on either side of the vessel, and are bolted to the base with the blind holes on the face of the pump motor. This allows the removable tube component of the pump to be easily removed for replacement of tubing or general maintenance or cleaning.

Next, the sensor packaging is mounted to the bottom side of the base after being assembled itself with the necessary LEDs and Photodiodes and filter as detailed in Section 7.2.3. The use of the sensor package as the locating feature for the vessel reduces the variability on the exact location of the trenches relative to the sensors.

Finally, the vessel heater is “clicked” into place after assembly with the necessary insulating and heating elements by rotating the vessel clockwise and forcing the sleeve into the compliant latches that will retain the heater.

7.2.2 Vessel Heater

The vessel heater heats the vessel to the initial temperature of the experiment, and then maintains the necessary temperature throughout the rest of the experiment. In order to accomplish consistent heating results, the heating sleeve will clamp around the vessel using a latch made of rubber or some other compliant material. This clamping action allows for a significantly better connection between the vessel and the heating pad and has the added benefit of adding some damping to the vessel, which may experience vibrations due to the mixing occurring within. The rubber latch remains attached permanently to the right latch, and is removed from the leftmost latch when a user removes or inserts the vessel. The force of the latch opening

or closing reacts into the solid side of the hook holding the heater in place, not the compliant side of the hook where the heater was inserted during assembly, preventing the heater from coming loose accidentally, or wearing the hook out over time.

7.2.3 Sensor Packaging

Sensors are packaged around the trenches of the bioreactor. They must hold the relevant LEDs and photodiodes to allow for noninvasive sensing of the conditions inside the reaction vessel.

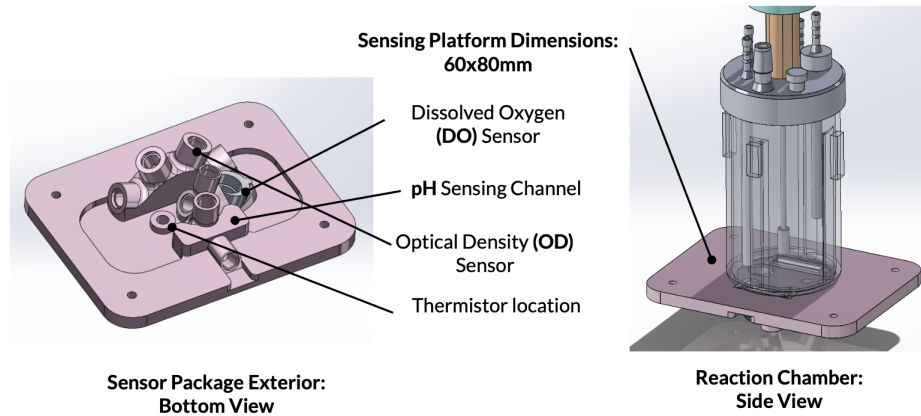


Figure 76: Overview of sensor packaging on the bottom of the disposable vessel. The four sensors implemented are Dissolved Oxygen (DO), pH, Optical Density (OD), and Temperature.

The geometries of each individual sensor package was informed by the requirements of the sensors. Each sensing package includes the mounts for the appropriate LEDs and photodiodes retained at the correct angles from each other. For further reading about the positioning of the LEDs and the photodiodes refer to Section 4.

8 Bill of Materials

We prepared a Bill of Materials to quantify that we met our design requirement of designing a bioreactor that costs less than \$1,000. In total, our bioreactor cost is \$838.50. Will format to look nicer. Some white paper examples have really nice BOMs.

Table 13: Bill of Materials

#	Subsystem	Category	Component Name	Company	Part #	Qty.	Cost per	Total Cost	Link
1	SECS	pH Sensing	LED	Mouse	521-9704F	1	\$0.67	\$0.67	Link
2	SECS	pH Sensing	Photodiode	Mouse	SFH 203	2	\$0.78	\$1.56	Link
3	SECS	OD Sensing	LED	Mouse	521-9704F	1	\$0.67	\$0.67	Link
4	SECS	OD Sensing	Photodiode	Mouse	SFH 21.3 FA	3	\$0.60	\$1.80	Link
6	SECS	DO Sensing	LED	Thorlabs	LED625E	1	\$6.87	\$6.87	Link
7	SECS	DO Sensing	Filter	Edmund Optics	Hoya R64	1	\$32.00	\$32.00	Link
8	SECS	DO Sensing	Photodiode	Thorlabs	FDS100	1	\$16.40	\$16.40	Link
9	SECS	DO Sensing	Reference photodiode	Mouse	SFH 203	1	\$0.78	\$0.78	Link
10	SECS	Power Electronics	Wall Power Adapter	Amazon		1	\$9.98	\$9.98	Link
11	SECS	Temp Sensing	Thermistor			1	\$0.00	\$0.00	Link
12	SECS	Logic components	Raspberry Pi 5			1	\$60.00	\$60.00	Link
13	SECS	Logic components	Raspberry Pi Touch Screen	Sparkfun	LCD-13733	1	\$60.00	\$60.00	Link
14	SECS	Logic components	Sensor Routing PCB			1	\$20.00	\$20.00	n/a
15	TF	Agitation	Impeller			1	\$1.00	\$1.00	n/a
16	TF	Heating	Heating Pad			1	\$71.11	\$71.11	Link
17	TF	Heating	TIM			0.009	\$104.00	\$0.90	Link
18	TF	Motors/Pumps	Feed Inlet	Kamoer		1	\$121.00	\$121.00	Link
19	TF	Motors/Pumps	Main Output	Kamoer		1	\$121.00	\$121.00	Link
20	TF	Motors/Pumps	Acid Input	Kamoer		1	\$121.00	\$121.00	Link
21	TF	Motors/Pumps	Base Input	Kamoer		1	\$121.00	\$121.00	Link
22	TF	Motors/Pumps	Stirring motor			1	\$13.95	\$13.95	Link
23	ST	Vessel	Membrane			1	\$22.00	\$22.00	
24	ST	Bioreactor Structure	Check Valve			1	\$10.00	\$10.00	Link
25	ST	Bioreactor Structure	Tubing			1	\$15.00	\$15.00	
26	ST	Bioreactor Structure	Bolts n shit			1	\$10.00	\$10.00	
27	ST	Gas Box	solenoid valve			1	\$40.00	\$40.00	Link
28	ST	Gas Box	Barbed fitting			1	\$10.00	\$10.00	Link
29	ST	Gas Box	Quick Connect (1/4in OD)			1	\$15.00	\$15.00	Link
30	ST	Gas Box	Tubing			1	\$15.00	\$15.00	Link
31	ST	Gas Box	Flow meter			3	\$110.00	\$330.00	Link

9 Future Work

9.1 Remaining Risks

There are a few key risks in this design that compromise the success of this product.

The highest risk issue is the success of the non-invasive sensing. The ruthenium-based layer and the polyaniline-based layer are based off of research done under very specific conditions and the conditions we've designed our product to be in are slightly different. To be more specific, the gap between the photodiode and the LED is larger than in research. We don't know yet to what extent this is a critical failure of the product until we make our own layer and test it. Throughout the course of the class we've done lab work creating these layers in an attempt to test them ourselves, but have yet to come to any conclusions. We hope to continue testing these layers to confirm the optical sensing will work as expected.

Another high risk in this design is the longevity of our sensors and their calibration. Even with good calibration methods, the sensors will eventually degrade and we currently do not know when this will happen. These kinds of tests require time or high levels of experience which we have neither of. We can make estimates based off of other uses of the same components, but given the large amount of uses from the user, we can't be sure of these numbers.

Below in Figure 77, a risk matrix from our Sponsor Presentation is given displaying three important risks and where they land on their likelihood and consequence.

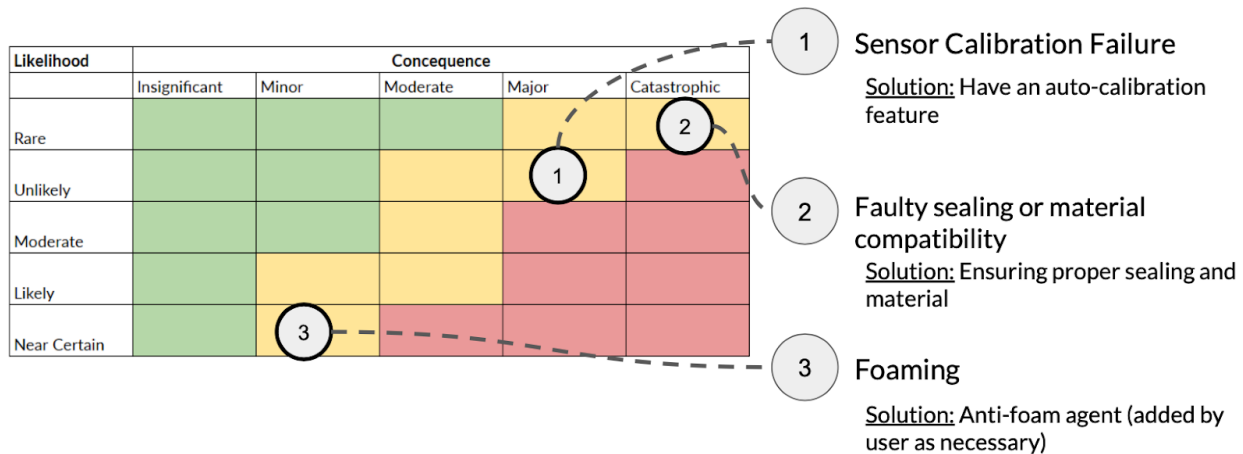


Figure 77: Risk Matrix of NIMBLE's implementation.

9.2 Remaining Design Work

The goal of this product is to fulfill as many needs as possible to serve as a general purpose bioreactor. One need that was not met due to being discovered too late in the design process was a solution for foaming within bioreactors. Foaming in bioreactors occurs when gas bubbles accumulate at the liquid surface faster than they decay, forming a stable foam layer. This phenomenon is common in many bioprocesses, including the production of antibiotics, vaccines, and yeast fermentation. Typically, users of bioreactors have an anti-foaming agent that reduces the foaming in their small-scale bioreactors. However, the implementation of the foaming-agent is very primitive and often causes problems. Bioreactors that are left running for long periods of time sometimes get contaminated because during the night, the foaming increases too much and floods the entire system. The only solution to reduce foam is to have someone present to monitor it and manually add a foaming agent. In the future, we'd like to implement a system that automatically detects foaming and adds the agent autonomously.

Our sensor system currently is a bundle of several LEDs and photodiodes, but we believe that this could be packaged much more effectively and possibly even reduced to a single LED and photodiode. There is a demand and interest in such small packaging because it would reduce space in the bioreactor and also reduce

likelihood of failure. Such a design would be extremely innovative and would likely need to be patented if proven successful.

9.3 Remaining Testing

The primary components of the system that require testing are sensors and the control systems.

Sensors still lack the confirmation that the optical sensing will work as expected. Although we expect that the design will work, we can also expect some unforeseen parameters that we will have to adjust for after testing. Optical sensors in particular can be very difficult to make reliable as they are very sensitive and are difficult to calibrate.

Our control scheme has been designed with many parameters kept in mind to assure it's as efficient as possible. However, it's possible that the process of simulation to real life is much different than we expect. Errors in our calculations regarding our control scheme likely aren't critical, but after testing we can make more decisions on how to adjust our parameters and better design a controller for our needs.

10 Acknowledgments

Throughout this project, this team received significant help and guidance from various sources. We would like to thank Professor Douglas Hart, Juergen Schoenstein, Jared Berezin, Jessica Lam, and Rohan Sanghai for their in-class guidance and support. We would like to thank Todd Thorsen for his continued support and technical mentorship in the project. We would also like to thank our outside sources such as Yuexuan Zu (Vincent), Vanessa Kitova, Audrey Chen, Ginkgo Bioworks, and Dr. AJ Perez.

11 References

- [1] S. Balasubramanian, A. K. Skidmore, Y. F. Wiersma, R. Darvishzadeh, and A. J. Comber. Does landscape composition influence the accuracy of land cover change detection? *Measurement*, 61:1–8, 2014.
- [2] Veerakiet Boonkanokwong, Brenda Remy, Johannes G. Khinast, and Benjamin J. Glasser. The effect of the number of impeller blades on granular flow in a bladed mixer. 302:333–349.
- [3] Simone Brethauer and Charles E. Wyman. Review: Continuous hydrolysis and fermentation for cellulosic ethanol production. *Bioresource Technology*, 102(20):9534–9542, 2011.
- [4] CYTENA. C.nest automated cell culture system, 2024.
- [5] Balaji Ganesh A. Deepa, N. Sol-gel based portable optical sensor for simultaneous and minimal invasive measurement of ph and dissolved oxygen. *Measurement*, 59:337–343, 2015.
- [6] Mojtaba Aghajani Delavar and Junye Wang. Bioreactor concepts, types, and modeling. In *Advanced Methods and Mathematical Modeling of Biofilms*, pages 195–245. Academic Press, 2022.
- [7] Oxford English Dictionary. fluorescence (n.), 2024.
- [8] Engineers Edge. Convective heat transfer coefficients table chart, 2024.
- [9] Essex Parts. Teknofibra 2mm flexible thermal barrier, 2024.
- [10] I. Fort, T. Jirout, F. Rieger, R. Allner, and R. Sperling. Study of the blending efficiency of pitched blade impellers. 41(6):7–13.
- [11] Richard K. Grenville, Jason J. Glacomelli, Gustavo Padron, and David A.R. Brown. Mixing: Impeller performance in stirred tanks. pages 46–55.
- [12] DeVincentis B. Hanspal, N. and J. A. Thomas. Modeling multiphase fluid flow, mass transfer, and chemical reactions in bioreactors using large-eddy simulation. *Engineering in Life Sciences*, 23(2):e2200020, 2022.
- [13] Bojan Isailovic, Byron Rees, and Michael Kradolfer. Fluid dynamics of a single-use, stirred-tank bioreactor for mammalian cell culture.
- [14] JoVE. Operation of a benchtop bioreactor, September 2013. DOI: 10.3791/50582-v.
- [15] Munna Kumar, Durga Prasad, Balendu Shekher Giri, and Ram Sharan Singh. Temperature control of fermentation bioreactor for ethanol production using imc-pid controller. *Biotechnology Reports*, 22:e00342, 2019.
- [16] Sergio Lucia and Felix Fiedler. Basics of model predictive control, 2023.
- [17] M. Ghougali. Various stages of nucleation and growth of thin films, 2019.
- [18] Brenna Norton-Baker Mauro Lua Harrison Steel Mackenzie C. R. Denton, Natasha P. Murphy and Gregg T. Beckham. Integration of ph control into chi.bio reactors and demonstration with small-scale enzymatic poly(ethylene terephthalate) hydrolysis. 63(13):1599–1607.
- [19] MatWeb. Overview of materials for polypropylene, molded, 2024.
- [20] National Semiconductor. 5A Low Dropout Positive Regulators, June 2005.
- [21] Newark. Gst60a12-p1j ac/dc power supply, ite, 1 output, 60 w, 12 v, 5 a, 2024.
- [22] Stefano Pineda. Sol gel process - final project in materials processing for micro- and nano-systems, December 2022.

- [23] Pioreactor. Features, 2024.
- [24] Pioreactor. Optical density, normalization, and growth rates, 2024.
- [25] Pioreactor. Pioreactor: The affordable bioreactor, 2024.
- [26] Pioreactor. Running a self-test, 2024.
- [27] PrasadLab. Synthesis of polyaniline sensors, March 2023.
- [28] Michael F. Robbins. Op-amp transimpedance amplifier, 2024.
- [29] Nicholas Rott and W. S. Lewellen. Boundary layers in rotating flows. Technical Report ATN-64(9227)-6, Aerospace Corporation, El Segundo, California, September 1964.
- [30] Sartorius. Ambr 250 modular technical specification, 2022.
- [31] Sartorius. Biostat b: The multi-talented bioreactor for research and development, 2022.
- [32] ScienceDirect. Optical density, 2024.
- [33] Scientific Bioprocessing Inc. A comparison between optical density and backscatter light, 2024.
- [34] Space Academy. Space communications calculator, 2024.
- [35] Dupont F Redouté JM Stoukatch S, Debliquy M. Low-cost optical ph sensor with a polyaniline (pani)-sensitive layer based on commercial off-the-shelf (cots) components. *Micromachines (Basel)*, 14(12):2197, 2023.
- [36] Roland B. Stull. *An Introduction to Boundary Layer Meteorology*. Kluwer Academic Publishers.
- [37] Prof. Thompson. *3.44 Materials Processing for Micro-Nano Systems*. Massachusetts Institute of Technology. Lecture: CVD.
- [38] James. A Tindall, Edwin P. Weeks, and Michael James Friedel. Part 2: A field study of enhanced remediation of toluene in the vadose zone using a nutrient solution. 168(1):359–389.
- [39] G. Paul Willhite. *Handbook of Natural Gas Transmission and Processing*. Elsevier, 2012.
- [40] Jingye Yang, Huzefa Dungrawala, Hui Hua, Arkadi Manukyan, Lesley Abraham, Wesley Lane, Holly Mead, Jill Wright, and Brandt L. Schneider. Cell size and growth rate are major determinants of replicative lifespan. 10(1):144–155.
- [41] Hai Zheng, Po-Yi Ho, Meiling Jiang, Bin Tang, Weirong Liu, Dengjin Li, Xuefeng Yu, Nancy Kleckner, Ariel Amir, and Chenli Liu. Interrogating the escherichia coli cell cycle by cell dimension perturbations. 113(52):15000–15005.
- [42] Yong Zhou, Li-Rong Han, Hong-Wei He, Bu Sang, Dai-Lin Yu, Jun-Tao Feng, and Xing Zhang. Effects of agitation, aeration and temperature on production of a novel glycoprotein GP-1 by streptomyces kanasenisi ZX01 and scale-up based on volumetric oxygen transfer coefficient. 23(1):125.

A Thermodynamics Calculations MATLAB Script

```
1 r_in_wall = 0.02; %m
2 r_out_wall = r_in_wall + 0.002; %m
3 r_in_heater = r_out_wall; %m
4 r_out_heater = r_in_heater + 0.001778; % m
5 r_in_insulation = r_out_heater; % m
6 r_out_insulation = r_in_insulation + 0.002 %m
7 r_in_clamp = r_out_insulation %m
8 r_out_clamp = r_in_clamp + 0.002 %m
9 r_in_structure = 0.022; %m
10 r_out_structure = r_in_structure + 0.010; %m
11
12 H_heater = 0.0254; %m
13 H_vessel = 0.08 - H_heater; %m
14
15 k_nylon = 0.14; %W/(m*C) Nylon12
16 k_heater = 0.2; %W/(m*C) Silicone Rubber
17 k_insulation = 0.026; %W/(m*C) Teknofibra 2mm
18
19 heated_SA = 2*pi*r_out_clamp*H_heater; %m^2
20 unheated_SA = 2*pi*r_out_structure*H_heater; %m^2
21 h_air = 50; %W/(m^2*C)
22
23 R_wall_heated = log(r_out_wall/r_in_wall)/(2*pi*k_nylon*H_heater) %C/W
24 R_heater = log(r_out_heater/r_in_heater)/(2*pi*k_heater*H_heater) %C/W
25 R_insulation = log(r_out_insulation/r_in_insulation)/(2*pi*k_insulation*H_heater) %C/W;
26 R_clamp = log(r_out_clamp/r_in_clamp)/(2*pi*k_nylon*H_heater) %C/W;
27 R_air_heated = 1 / (h_air * heated_SA) %C/W
28 R_heated_tot = R_wall_heated + R_heater + R_clamp + R_air_heated %C/W
29 R_wall_unheated = log(r_out_wall/r_in_wall)/(2*pi*k_nylon*H_vessel) %C/W
30 R_air_unheated = 1 / (h_air * unheated_SA) %C/W
31 R_unheated_tot = R_wall_unheated + R_air_unheated %C/W
32
33 T_water = 50; %C
34 T_ambient = 20; %C
35 D_T = T_water - T_ambient; %C
36
37 Q_dot_heated = D_T/R_heated_tot; %W
38 Q_dot_unheated = D_T/R_unheated_tot; %W
39 Q_dot_tot = Q_dot_heated + Q_dot_unheated %W
```

B Shear Calculations

Assuming a relatively small vertical shear in steady state conditions (i.e., $\tau_{rz}, \tau_{\theta z} \ll \tau_{r\theta}$), circumferential shear warrants the strongest consideration given that the highest tangential velocity occurs farthest from the rotating center. The axisymmetric boundary layer flow is visualized in Figure B-1.

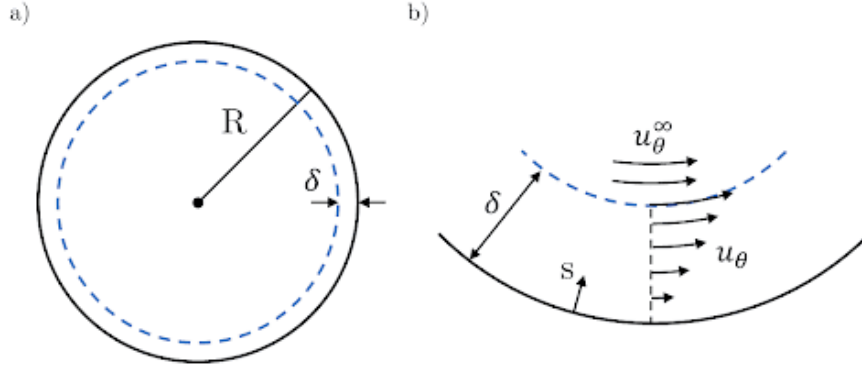


Figure B-1: (a) Axisymmetric boundary layer flow inside a cylinder, where δ is the boundary layer width. (b) Enlarged visualization of boundary layer development.

The maximum tangential velocity is treated here as u_θ^∞ , as indicated in Equation B-1.

$$u_\theta(r = R - \delta) = u_\theta^\infty \approx \omega R \quad (\text{B-1})$$

where ω is the stirring speed.

Equations B-2 and B-3 delineate boundary layer formulation for axisymmetric boundary layer flow inside a cylinder [29].

$$\tau = 0.225\rho(U^2 + V^2) \left(\frac{\nu}{\sqrt{U^2 + V^2}} \right)^{1/2} \quad (\text{B-2})$$

$$\tau_{r\theta} = \tau \cdot \frac{\nu}{\sqrt{U^2 + V^2}} \quad (\text{B-3})$$

At steady state, we assume,

$$U \approx 0 \left[\frac{m}{s} \right]$$

$$V = u_\theta^\infty \approx \omega R$$

Mammalian cells cannot withstand shear forces above 20 Pa. Implementing Equations XI and XII provide the stirring speed associated with 20 Pa, as denoted below.

$$\tau_{r\theta} \leq (\tau_{r\theta})_{max} = 0.225\rho\omega^{3/2}R^{3/2}\nu^{1/4}$$

$$\omega \leq \omega_{max} = 14.6 \frac{\text{rad}}{\text{s}} \approx 140 \text{ RPM}$$

The rate 140 RPM represents the maximum stirring speed that can be imposed on mammalian cells.

C Sensors Calculations MATLAB Script

```
1 % Plot the curve
2 figure;
3 plot(X, Y, 'b-', 'LineWidth', 2);
4 title('LED625E Spatial Radiation Distribution');
5 xlabel('Angular Displacement (Degrees)');
6 ylabel('Relative Intensity');
7 grid on;
8
9
10 idx = find(X >= 0 & X <= 15);
11
12
13 % Extract data points within the desired range
14 x_range = X(idx);
15 y_range = Y(idx);
16 % Calculate the integral under the curve
17 integral_value_total = trapz(X, Y);
18 integral_value_15 = trapz(x_range, y_range);
19
20
21 % Display the integral value
22 text_str = sprintf('Integral: %.4f', integral_value_total)
23 %text(0.7, 0.9, text_str, 'Units', 'normalized', 'FontSize', 12);
24 text_str = sprintf('Integral: %.4f', integral_value_10)
25 %text(0.7, 0.9, text_str, 'Units', 'normalized', 'FontSize', 12);
26 percent_str = sprintf('Emitted within 15 deg: %.2f%%', integral_value_15/
    integral_value_total*100)
27 % Display the integral value on the plot
28 text_x_position = 30; % X position for displaying text (adjust as needed)
29 text_y_position = 0.5; % Y position for displaying text (adjust as needed)
30 text(text_x_position, text_y_position, percent_str, 'FontSize', 12, 'Color', 'k');
31
32
33 % Calculate and plot the area under the curve
34 hold on;
35 area(X, Y, 'FaceColor', 'b', 'FaceAlpha', 0.3);
36 hold on;
37 area(x_range, y_range, 'FaceColor', 'r', 'FaceAlpha', 0.3);
38 legend('Curve', '> 15\circ', '< 15\circ');
```